Optimal Power-Sharing Control for MTDC Systems

by

Khaled Alshammari

A thesis
presented to the University of Waterloo
in fulfillment of the
thesis requirement for the degree of
Master of Applied Science
in
Electrical and Computer Engineering

Waterloo, Ontario, Canada, 2019

Author's Declaration

I hereby declare that I am the sole author of this thesis. This is a true copy of the thesis, including any required final revisions, as accepted by my examiners.

I understand that my thesis may be made electronically available to the public.

Abstract

Power systems have been developing over the past few decades, especially in terms of increasing efficiency and reliability, as well as in meeting the recent rapid growth in demand. Therefore, High Voltage Direct Current (HVDC) systems are considered to be one of the most promising and important contenders in shaping the future of modern power systems. A number of trends demonstrate the need to implement Multi-terminal Direct Current (MTDC) systems, including the integration into the conventional grid of renewable energy resources such as photovoltaic (PV) and offshore wind farms. The transmission of power from or to remote areas, such as the North Sea in Europe, is another initiative that is required in order to meet the high demand for power. The interconnection between countries with different levels of frequencies over a long distance is a fundamental application of HVDC grids as well as hybrid AC/DC transmission systems. The industry has also played an essential role in the accelerated progress in power electronics devices regarding cost and quality. Consequently, Voltage Source Converter based-High Voltage Direct Current (VSC-HVDC) systems has recently attracted considerable attention in the research community. This type of HVDC systems has a significant advantage over the classic Current Source Converter based-HVDC (CSC-HVDC) in terms of the independent control of both active and reactive power. Since VSC-HVDC is now being implemented in various applications, this requires a close examination of the behavior of both the economic and operational issues of both VSC-HVDC stations and MT-HVDC systems.

This thesis proposes an optimal power-sharing control of MT-HVDC systems using a hierarchical control structure. In the proposed control scheme, the primary control is decentralized and operated by a DC voltage droop control. This method regulates the voltage source converters (VSCs) and guarantees a stable DC voltage throughout the system even in the presence of sudden changes in power flow. A centralized optimal power

flow (OPF) is implemented in the secondary control to set the droop gains, and voltage settings in order to fulfil a multi-objective function. This aims at minimizing the losses in DC grid lines and converter stations by an optimization algorithm, namely Semidefinite Programming (SDP). Therefore, an optimal power-sharing result is achieved taking into consideration the losses of both transmission lines and converters, as well as failure intervals of the system. The proposed control scheme was tested on a modified CIGRE B4 DC grid test system based on the PSCAD/EMTDC and MATLAB in which the primary control was designed and simulated in the former, whereas the latter was used to run the SDP algorithm.

Acknowledgements

First, praise to Allah who guided and blessed me throughout my work and my whole life.

I would like to express my sincere gratitude and appreciation to my supervisor, Dr. Ramadan El-Shatshat, for his guidance, support and patience during my research and writing of this thesis.

My special thanks and endless gratitude go to my brother, friend, and mentor, Hasan Alrajhi Alsiraji, who has been with me since day one, helping me with everything.

I would like to express my warmest thanks to Ms. Sibel Kiamil for letting me to be part of her family.

My deepest thanks and profound gratitude to my wonderful family for their prayers, patience and encouragement. None of this would be possible without them.

Dedication

This thesis is dedicated

To my mother, Wadha

To my father, Mubarak

To my brother, Abdulaziz

To my sister, Reem

To my young brother, Hussam

Table of Contents

List of Tables

List of Figures

Nomenclature

AC	Alternating Current
DC	Direct Current
HVAC	High Voltage Alternating Current
HVDC	High Voltage Direct Current
LCC	Line Commutated Converter
MTDC	Multi-terminal High Voltage Direct Current
OPF	Optimal Power Flow
RES	Renewable Energy Sources
SDP	Semidefinite Programming
VSC	Voltage Source Converter

Chapter 1

Introduction

1.1 Preamble

The integration of Renewable Energy Sources (RESs) into conventional AC grids has induced a revolution and a significant shift in the direction of power systems in recent years. This trend was driven by two major factors, namely the rapid growth of demand and a higher level of greenhouse gas emissions into the atmosphere. Offshore wind farms and photovoltaic energy are the most promising and widely-used RES types around the world, and the efficiency of these sources mainly depends on where and how they are installed [3]. In 2018, the European Union (EU) installed more wind energy capacity than any other form of electricity generation. Solar power electricity generation has increased rapidly in recent years in the EU-27 countries, doubling from 2007 to 2017 from 0.7% to 12.3% of net electricity production [1] [4].

Consequently, High-Voltage Direct Current (HVDC) systems are considered to be a substantial solution to the high penetration of RES due to several reasons. The location of

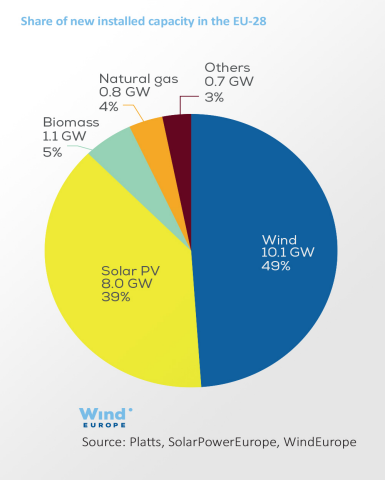

Figure 1.1: Wind and solar energy shares in Europe [1]

wind farms, such as generation projects in the North Sea in Europe, has stimulated the need to transmit power from or to remote areas over long distances with the aim of minimizing losses [5]. The advancements of power electronic devices in industry and technology have led to the expansion of HVDC systems in terms of quality and cost. In order to meet the increasing demand of various countries in the same region, HVDC transmission systems are used to interconnect between asynchronous AC systems with different frequencies, unlike a traditional AC connection. An HVDC connection is an efficient and economical alternative in terms of employing solar and wind energy due to minimizing power transmission losses and voltage conversion stages [6–9].

1.2 MT VSC-HVDC Systems

Multi-terminal HVDC-VSC based systems are the ultimate choice regarding the scope of this thesis. This was determined according to several aspects, starting from HVDC over

high voltage alternating current (HVAC), VSC-HVDC over LCC-HVDC, and MTDC over a point-to-point HVDC connection.

As the primary starting point, high voltage (HV) is the most common type in transmission systems because of the reduction of line losses compared to medium voltage (MV).

- From a power flow control perspective, an HVDC connection can control the power flow direction and magnitude by changing either the voltage polarity or the current direction, while an HVAC connection needs particular equipments, such as unified power flow control (UPFC) in order to change the power flow. Transmission lines in HVDC systems do not have distance limits nor reactive power loss in contrast to HVAC where transmission lines have capacitive and inductive impedances. HVDC systems also have the ability to carry a higher amount of power for any size of conductor.

- From a stability perspective, HVAC is more likely to be unstable compared to HVDC systems with regard to all the operational and thermal limits whereas HVDC systems improve stability for their connection and also for interconnecting AC grids.

- From an economical perspective, HVDC overhead lines are more cost effective than HVAC when the transmission exceeds certain distance. HVDC systems can deliver power to areas where the demand is high and new generators cannot be installed. They can also increase the capacity of existing AC transmission systems. HVDC connections among AC systems do not require synchronization and also have a lower number of voltage conversion stages in comparison to HVAC connections [10–12].

Classical HVDC systems primarily depend on line commutated converters (LCCs) which are based on thyristors. Notwithstanding the aforementioned advantages in the previous section, LCCs:

- Lack the ability to reverse the current direction.
- Require and consume reactive power
- Supply only active loads.
- Have a high possibility of commutation failure [5, 13, 14].

These limitations, alongside the overall cost of LCCs, have introduced the Voltage Source Converter (VSC) into the field of HVDC systems. VSCs, which are based on an insulated gate bipolar transistor (IGBT) with an anti-parallel diode, are self-commutated converters, unlike LCCs [15]. VSCs can independently control active and reactive power, and have the ability to reverse power flow direction without the need to change the DC voltage polarity [16, 17].

As previously mentioned, HVDC grid applications include the transmission of power over long distances and interconnection among asynchronous AC systems. These applications demand a high level of power which usually cannot be met by a one or two-terminal HVDC system, also known as classic HVDC systems. Hence, MTDC VSC-based grids have the edge over the aforementioned HVDC structures in regards to cost, reliability, and ability to handle expected expansion in distribution systems to meet the demand growth [18]. The flexibility to control the power flow within the grid is a significant advantage that is profoundly needed by power electricity markets and power operators. Power quality can be improved by controlling the AC system voltage through the reactive power of VSC-HVDC

stations. Short circuit faults on the AC side have a negligible effect on the DC side because the converter can operate regardless of AC sources [19].

1.3 Thesis Motivation

Power grids were dominated by AC transmission systems for the past few decades until the rise in implementing renewable resources into traditional AC networks. This rise caused DC grids to gain considerable attention in the research community over the last few years as the demand of power has had a rapid and positive upward slope. The challenges of integrating distributed generations (DGs) have also incited this interest with the boost in the industry of power electronics, especially VSCs. One of the most important applications of MTDC systems is transmitting power that is generated from offshore wind farms or onshore AC systems. As a result, MTDC grids have no reactive power compensation and fewer of the conversion steps which are needed to collect a large amount of power from remote areas. This amount of power has to be shared among a multi-terminal HVDC system based on a desired share in order to: minimize grid losses; increase penetration of RESs; and operate within the system limits such as voltage regulation limits, rated power of VSCs and the capacity of lines. Power sharing among multi-terminal HVDC systems has been investigated in various studies in order to fulfill the previous objectives. However, the losses of both lines and converters have not been considered. Therefore, this thesis proposes an optimal power sharing control of MTDC systems based on droop control and Optimal Power Flow (OPF) as the primary and secondary control, respectively.

1.4 Thesis Contributions

This thesis has many research objectives which can be summarized as follows:

- To study and evaluate the behaviour of the voltage source converter in terms of the working principle, power flow, and configurations.
- To use and analyze various control techniques to operate a detailed VSC model in an MTDC system.
- To introduce a new hierarchical control scheme which includes a droop voltage control in the primary level and using Semidefinite Programming (SDP) as a secondary control technique to solve the OPF problem.
- To optimize the power sharing process among MTDC terminals by taking into consideration the losses of lines and converters.
- To test and validate the proposed control technique using a modified CIGRE B4 DC grid test system.

1.5 Thesis Organization

The organization of the rest of this thesis is described as follows:

- Chapter 2 presents the background and a literature review of the voltage source converter (VSC) in terms of the working principle, design, and the power flow model. In addition, control techniques of the VSC are described and analyzed as well as all of the different configurations of VSC stations in HVDC systems.

- Chapter 3 provides an overview of power sharing control in MT-HVDC VSC-based systems. An up-to-date literature survey is conducted regarding the proposed control scheme, and its formulation is explained through the chapter.

- Chapter 4 illustrates the simulation results of the proposed scheme in which a number of cases are presented to show the verification of the control strategy in MTDC systems.

- Chapter 5 presents the conclusion of the thesis and suggests future work in the area.

Chapter 2

Modelling and Control of MTDC VSC-based Systems

This chapter presents a general overview and important aspects of MTDC VSC-based systems. The concept of the VSC is first addressed along with its operation process. Secondly, a description and explanation of the control design and modelling of the VSC are provided. Finally, different HVDC-VSC configurations are investigated and compared.

2.1 VSC Station

In order to explain the VSC concept, the topology of both DC-DC-converters and buck and boost converters should be introduced since the VSC is a combination of both. Boost (step-up) and buck (step-down) DC-DC converters are shown in Figure 2.1, where it can be seen that they both have the same components, namely an inductance, diode, capacitor, and a switch, but in different structures. Switching control signals play a crucial part in the

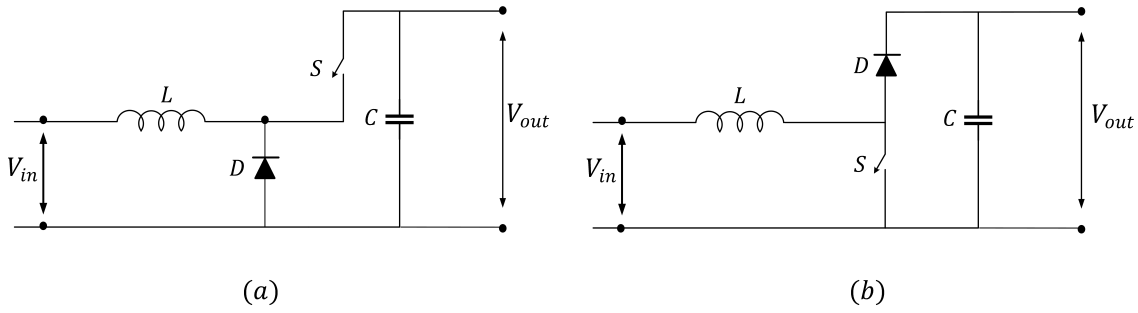

Figure 2.1: (a) Buck converter (b) Boost converters

operation of these converters since the current cannot be conducted unless the switches are forward biased. The output (V_o) and input (V_i) voltage is mainly controlled by a switching signal, called the switch duty ratio (D), which is defined as the ratio of the ON duration to the switching time period (T_{sf}) [20].

$$V_o = D_{on} V_{in} \tag{2.1}$$

$$V_o = (1 - D_{off}) V_{in} \tag{2.2}$$

$$D_{on} = \frac{T_{on}}{T_{sf}} \tag{2.3}$$

$$T_{sf} = T_{on} + T_{off} = \frac{1}{f_s} \tag{2.4}$$

where f_s is the switching frequency, and the relationships in Equation 2.3 and Equation 2.4 are shown in Figure 2.2.

A bidirectional DC-DC converter can be composed by incorporating the buck and boost converters since they have a unidirectional power flow. This combination of a bidirectional

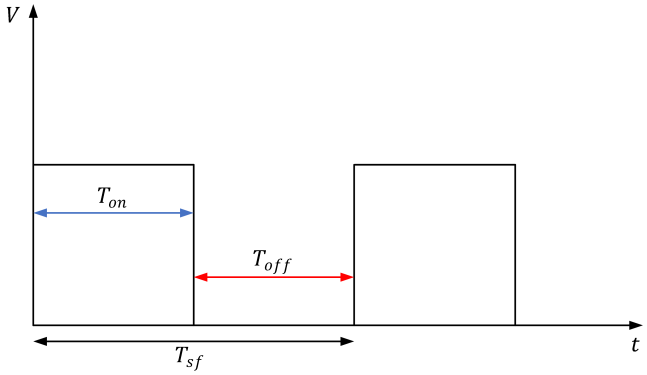

Figure 2.2: Switching ON and OFF states

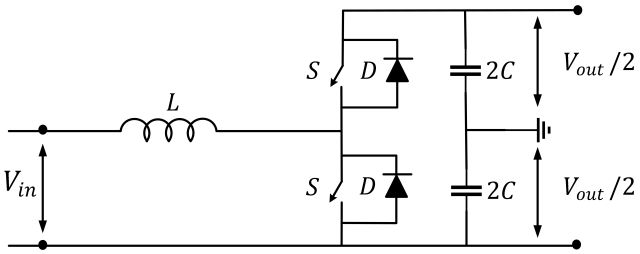

Figure 2.3: Half bridge converter

power flow converter requires an equality relationship between the input and output voltage as shown in the following equation:

$$V_o = D_{on}V_i = (1 - D_{off})V_i \tag{2.5}$$

Figure 2.3 demonstrates the new topology of combining buck and boost converters after splitting the DC capacitor into two, and the output voltage into two halves, which forms the design of a half bridge converter. Applying a sinusoidal pulse width modulation (PWM) to the bidirectional converter makes a half bridge single phase converter, and three of these converters connected in parallel constructs a three-phase bidirectional converter, namely a voltage source converter (VSC) as shown in Figure 2.4. As can be seen from

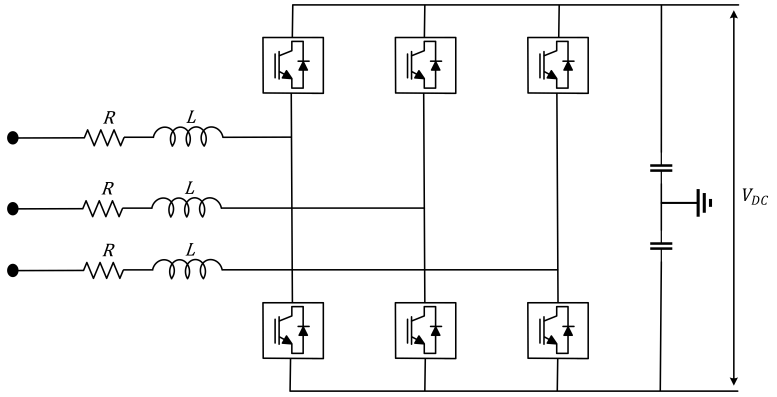

Figure 2.4: Voltage source converter

the name, the DC voltage polarity is fixed, which indicates that the power direction is controlled by the direction of the current.

The (IGBT) is one of the most important components of the VSC station due to its unique characteristics such as the ability to turn both ON and OFF, and including a controllable gate. The IGBT is a unidirectional switch that operates only when the current flows from the collector (C) to the emitter (E). The operation of this device combines the Bipolar Junction Transistor (BJT) in terms of the reduction of losses when turned ON, and the Metal Oxide Semiconductor Field Effect Transistor (MOSFET) in terms of the simplicity of gate drivers. The IGBT also has superiority over the other types of transistors in terms of switching speed and safe operating area. Parallel-connected IGBTs are required in order to meet high current levels since these devices are implemented in HVDC applications. Similarly, series-connected IGBTs are required to handle high voltage and power ratings alongside the minimization of losses [21].

Pulse Width Modulation (PWM) is used in VSC-HVDC systems to generate switching signals in order to control the gates of IGBTs in the converter. This occurs by comparing a sinusoidal control signal V_{cont} with a triangular waveform V_{tri} to produce an output voltage

waveform that is independent from the AC system. The ratio of the peak value of V_{cont} and the peak value of V_{tri} is the definition of modulation index M [20].

$$M = \frac{V_{cont}}{V_{tri}} \tag{2.6}$$

As a result of comparing both signals V_{cont} and V_{tri}, duty cycles of the switching signals in which the upper switches are ON when the control signal is greater than the triangular waveform, and the lower switches are ON when the triangular waveform is greater than the control signal.

$$\begin{aligned} V_{cont} > V_{tri} &\longrightarrow S_{upper} \text{ are } ON \\ V_{cont} < V_{tri} &\longrightarrow S_{lower} \text{ are } ON \end{aligned} \tag{2.7}$$

The VSC-HVDC station has a basic operation principle, which is that each converter in the system is represented by the AC voltage source that is connected to the AC transmission lines via series impedances. In this scenario, the VSC acts as a fast controllable synchronous machine with an output phase voltage expressed by:

$$V_{out} = \frac{1}{2} V_{dc} M sin(\omega t + \delta) \tag{2.8}$$

where ω is the fundamental frequency, and δ is the phase shift of the output voltage. The variables M and δ in the previous equation are independently controlled using PWM to set the voltage magnitude and phase angle. Thus, the voltage difference between the converter and the AC grid causes the power transfer, and can be controlled by these variables. The phase angle δ regulates the flow of active power; whereas, the reactive power is governed by the magnitude of AC voltage [22].

$$P = \frac{V_{grid} V_{conv}\, sin\delta}{X} \tag{2.9}$$

$$Q = \frac{V_{grid}(V_{grid} - V_{conv}\, cos\delta)}{X} \tag{2.10}$$

2.2 VSC Design

A two-level VSC with sinusoidal PWM and high voltage levels is employed in this thesis, and its modelling consists of a single IGBT and diode. The IGBT is a completely-controlled device that can only conducts the current in one direction, so an anti-parallel diode is connected in order to allow the current to flow to the opposite direction. The main components of a VSC station are listed as follows:

1. Transformer.

   Because they are located between the main AC grid and the converter, transformers either step up or step down the voltage to an acceptable level for the converter. Moreover, in this application, transformers usually have a simple connection, e.g. two windings.

2. AC filter.

   The switching of IGBTs causes the AC voltage to include harmonics that need to be eliminated. Therefore, high-pass filters are installed to protect the AC system from any unexpected disturbances while in operation or communication, especially caused by high order harmonics.

3. Phase reactor.

   Phase reactors have the ability to regulate flowing-through currents that control the flow of active and reactive power. In addition, characteristics of both active and reactive power are set according to the reactor's voltage. Phase reactors can act as AC filters in terms of minimizing the currents' frequency harmonics due to the switching of the converter.

4. DC capacitors.

   Two capacitors, of the same size, are placed on the DC side in order to control power flow by acting as an energy storage, and to grant the off-current to flow in line with low inductance. This current may have some harmonics as a result of the switching process of the VSC leading to a potential DC voltage ripple. The design and size of these capacitors are determined by the anticipated level of both the DC voltage and its ripple. Disturbances, such as faults, in the AC side have to be considered in the design as well as the steady state of the system because these disturbances may cause oscillations and over-voltages in the DC side. A small size capacitor is implemented and represented by a time constant τ, which is the ratio between the energy stored in the capacitor at a rated DC voltage, and the apparent power of the VSC.

$$\tau = \frac{\frac{1}{2}CV_{dc}^2}{S} \tag{2.11}$$

   This time constant has the same value as the time consumed by the capacitor to charge from zero to the level of V_{dc} under the condition of the converter receiving power that is equal to the active power part of S [23].

2.3 VSC Power Flow Model

One of the main objectives of the VSC station is to link AC grids with DC grids especially in MTDC system applications. This connection occurs using a phase reactor and filter that are connected to the AC grid through a transformer that allows power to flow bidirectionally. The direction of power flow determines the VSC mode of operation in which the converter works as an inverter when the active power is delivered to the AC grid from the DC grid. In contrast, the VSC acts as a rectifier if the active power flows from the AC grid to the

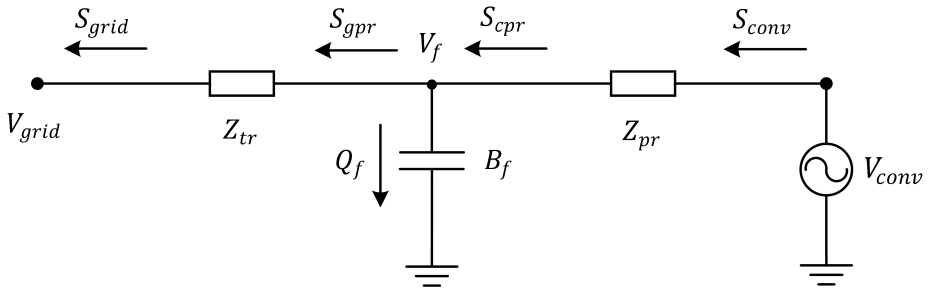

Figure 2.5: A single line diagram of a VSC

DC grid. The equivalent single phase model of the VSC is shown in Figure 2.5 where all the main components are illustrated with the directions of power flow. Starting from the converter side, the VSC is a controllable AC voltage source $V_{conv} = V_{conv}\angle\delta_{conv}$ as stated in section 2.1, followed by the phase reactor, which is donated by an impedance $Z_{pr} = R_{pr} + jX_{pr}$, while $1/Z_{pr} = G_{pr} + jB_{pr}$ is the admittance of the phase reactor. The susceptance B_f represents the low pass filter that is connected to the AC grid via a transformer with its impedance $Z_{tr} = R_{tr} + jX_{tr}$, and admittance $1/Z_{tr} = G_{tr} + jB_{tr}$. The voltage at the grid side is donated by $V_{grid} = V_{grid}\angle\delta_{grid}$, whereas the filter voltage is $V_f = V_f\angle\delta_f$. The equations of the active and reactive power at the AC grid side and the converter side are expressed, respectively, as [24]:

$$P_{grid} = -V_{grid}^2 G_{tr} + V_{grid}V_f\left[G_{tr}\,cos(\delta_{grid} - \delta_f) + B_{tr}\,sin(\delta_{grid} - \delta_f)\right] \tag{2.12}$$

$$Q_{grid} = V_{grid}^2 B_{tr} + V_{grid}V_f\left[G_{tr}\,sin(\delta_{grid} - \delta_f) - B_{tr}\,cos(\delta_{grid} - \delta_f)\right] \tag{2.13}$$

$$P_{conv} = V_{conv}^2 G_{pr} - V_f V_c\left[G_{pr}\,cos(\delta_f - \delta_c) - B_{pr}\,sin(\delta_{grid} - \delta_{conv})\right] \tag{2.14}$$

$$Q_{conv} = -V_{conv}^2 B_{pr} + V_f V_c\left[G_{pr}\,sin(\delta_f - \delta_c) + B_{pr}\,cos(\delta_{grid} - \delta_{conv})\right] \tag{2.15}$$

The power equations of the filter, and the reactive power of the lossless AC filter, are presented, respectively, as:

$$P_{gpr} = V_f^2 G_{tr} - V_f V_{grid}\left[G_{tr}\,cos(\delta_{grid} - \delta_f) - B_{tr}\,sin(\delta_{grid} - \delta_f)\right] \tag{2.16}$$

$$Q_{gpr} = -V_f^2 B_{tr} + V_f V_{grid} \left[G_{tr}\, sin(\delta_{grid} - \delta_f) + B_{tr}\, cos(\delta_{grid} - \delta_f) \right] \tag{2.17}$$

$$Q_f = -V_f^2 B_f \tag{2.18}$$

The active and reactive power equations of the phase reactor are:

$$P_{cpr} = -V_f^2 G_{pr} + V_f V_{conv} \left[G_{pr}\, cos(\delta_f - \delta_{conv}) + B_{pr}\, sin(\delta_f - \delta_{conv} \right] \tag{2.19}$$

$$Q_{cpr} = V_f^2 B_{pr} + V_f V_{conv} \left[G_{pr}\, sin(\delta_f - \delta_{conv}) - B_{pr}\, cos(\delta_f - \delta_{conv} \right] \tag{2.20}$$

2.4 VSC Control Techniques

The control aspect of VSC-HVDC systems can be summarized as the control of the transfer of energy between the input and output side. Specifically, the control of transferred power is the objective of VSC-HVDC systems with the ability to independently control active and reactive power.

A number of control techniques have been used for VSC-HVDC systems, two of which will be discussed since they are the most common methods.

2.4.1 Direct Power Control

Firstly, the Direct Power Control (DPC) technique implements predicated virtual flux vector for the control loop along with the instantaneous active and reactive power control loops. This strategy, which lacks PWM switching and inner current control loops, instead uses the instantaneous difference between the required and estimated values of active and reactive power for the switching process [25]. Accordingly, DPC is not a preferred control method in terms of the need for fast and instantaneous calculations, and the incapability of an independent power control.

2.4.2 Vector Control

Secondly, vector control has the ability to independently control active and reactive power especially for PWM converters. The vectors of both the current and voltage remain constant in steady state and, in the case of errors, a proportional integral (PI) controller is implemented. Axis transformations are being used by vector control in order to model three-phase systems as described in the following paragraph.

Vector control consists of a two-step transformation, starting from the three-phase stationary to the d-q rotating coordinate system with the aim of representing the quantities of AC voltages and currents. Clark transformation is first used to transform the three-phase vectors with a 120°phase shift into a two-phase (α - β) stationary system. The α-axis is aligned with the first phase a-axis, and the β-axis is placed vertically on the three-phase vectors, forming a 90° with the a-axis, as shown in Figure 2.6.

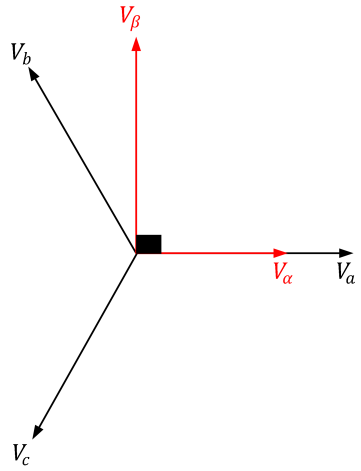

Figure 2.6: ABC, and α-β reference frames

The mathematical model of Clark transformation of voltages is explained in Equa-

tion 2.21 to Equation 2.24, and the same applies for currents.

$$V_a + V_b + V_c = 0 \tag{2.21}$$

$$\begin{aligned} V_\alpha &= V_a\, cos(0) + V_b\, cos(120) + V_c\, cos(120) \\ &= V_a\,(1) + V_b\left(-\frac{1}{2}\right) + V_c\left(-\frac{1}{2}\right) \end{aligned} \tag{2.22}$$

$$\begin{aligned} V_\beta &= V_a\, cos(90) + V_b\, cos(30) + V_c\, cos(150) \\ &= 0 + V_b\left(\frac{\sqrt{3}}{2}\right) + V_c\left(-\frac{\sqrt{3}}{2}\right) \end{aligned} \tag{2.23}$$

$$\begin{bmatrix} V_\alpha \\ V_\beta \end{bmatrix} = k \cdot \begin{bmatrix} 1 & -\frac{1}{2} & -\frac{1}{2} \\ 0 & \frac{\sqrt{3}}{2} & -\frac{\sqrt{3}}{2} \end{bmatrix} \cdot \begin{bmatrix} V_a \\ V_b \\ V_c \end{bmatrix} \tag{2.24}$$

If the value of k in Equation 2.24 equals $2/3$, as expressed in Equation 2.25, the voltage magnitude of α-β frame is equal to the voltage magnitude of the abc frame, and can be described as voltage invariant.

$$\begin{bmatrix} V_\alpha \\ V_\beta \end{bmatrix} = \frac{2}{3} \cdot \begin{bmatrix} 1 & -\frac{1}{2} & -\frac{1}{2} \\ 0 & \frac{\sqrt{3}}{2} & -\frac{\sqrt{3}}{2} \end{bmatrix} \cdot \begin{bmatrix} V_a \\ V_b \\ V_c \end{bmatrix} \tag{2.25}$$

However, if k has the value of $\sqrt{\frac{3}{2}}$ as derived in Equation 2.26, the power of the abc frame is equivalent to the power of the α-β frame, and this transformation can be called power invariant.

$$Gain = G = \sqrt{(1)^2 + \left(-\frac{1}{2}\right)^2 + \left(-\frac{1}{2}\right)^2} = \sqrt{\frac{3}{2}} \tag{2.26}$$

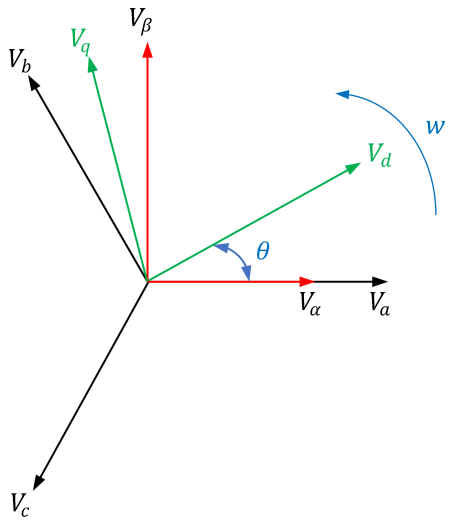

Figure 2.7: dq rotating frame

$$\begin{bmatrix} V_\alpha \\ V_\beta \end{bmatrix} = \sqrt{\frac{2}{3}} \cdot \begin{bmatrix} 1 & -\frac{1}{2} & -\frac{1}{2} \\ 0 & \frac{\sqrt{3}}{2} & -\frac{\sqrt{3}}{2} \end{bmatrix} \cdot \begin{bmatrix} V_a \\ V_b \\ V_c \end{bmatrix} \tag{2.27}$$

In the second stage, Park transformation is implemented to convert the stationary α-β to the synchronous rotating d-q frame based on a synchronous speed w, and the rotor angle between the d-axis and α-axis, which is donated by $\theta = wt$, as shown in Figure 2.7.

$$\begin{bmatrix} V_d \\ V_q \end{bmatrix} = \begin{bmatrix} cos\theta & sin\theta \\ -sin\theta & cos\theta \end{bmatrix} \cdot \begin{bmatrix} V_\alpha \\ V_\beta \end{bmatrix} \tag{2.28}$$

$$\begin{bmatrix} V_d \\ V_q \end{bmatrix} = \frac{2}{3} \cdot \begin{bmatrix} cos\theta & cos\left(\theta - \frac{2\pi}{3}\right) & cos\left(\theta + \frac{2\pi}{3}\right) \\ -sin\theta & -sin\left(\theta - \frac{2\pi}{3}\right) & -sin\left(\theta + \frac{2\pi}{3}\right) \\ \frac{1}{2} & \frac{1}{2} & \frac{1}{2} \end{bmatrix} \cdot \begin{bmatrix} V_a \\ V_b \\ V_c \end{bmatrix} \tag{2.29}$$

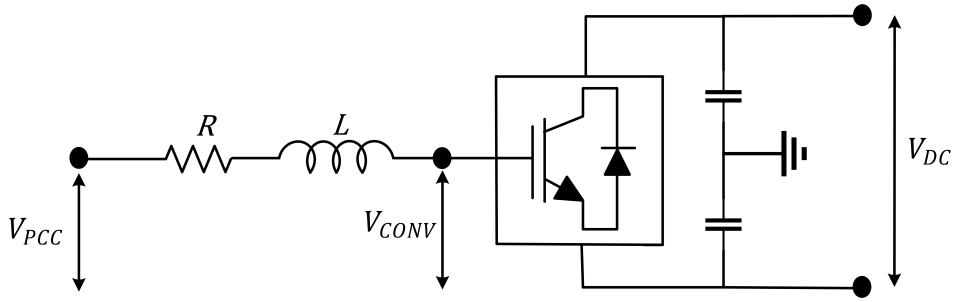

Figure 2.8: The VSC station

Therefore, vector control for a VSC requires a mathematical model in the dq frame, which begins by applying Kirchhoff's Voltage Law (KVL) between the converter station and the main AC grid, including converter input voltage V_{abc}^{conv}, resistance R, inductance L, and the grids' voltages V_{abc}^{grid} and currents i_{abc} in the abc frame, as depicted in Equation 2.30 and Figure 2.8.

$$V_{abc}^{grid} - V_{abc}^{conv} = R \cdot i_{abc} + L\frac{di_{abc}}{dt} \tag{2.30}$$

Based on Equation 2.29, the first term of Equation 2.30 will be:

$$\begin{aligned} V_d^{grid} &= \frac{2}{3}\left[V_a\, cos(\theta) + V_b\, cos(\theta - \frac{2\pi}{3}) + V_c\, cos(\theta + \frac{2\pi}{3})\right] \\ V_q^{grid} &= -\frac{2}{3}\left[V_a\, sin(\theta) + V_b\, sin(\theta - \frac{2\pi}{3}) + V_c\, sin(\theta + \frac{2\pi}{3})\right] \end{aligned} \tag{2.31}$$

And the second term of Equation 2.30 will be similar to the first:

$$\begin{aligned} V_d^{conv} &= \frac{2}{3}\left[V_a\, cos(\theta) + V_b\, cos(\theta - \frac{2\pi}{3}) + V_c\, cos(\theta + \frac{2\pi}{3})\right] \\ V_q^{conv} &= -\frac{2}{3}\left[V_a\, sin(\theta) + V_b\, sin(\theta - \frac{2\pi}{3}) + V_c\, sin(\theta + \frac{2\pi}{3})\right] \end{aligned} \tag{2.32}$$

The currents flowing through the inductance and resistance are expressed as follows:

$$\begin{aligned} i_d &= \frac{2}{3}\left[i_a\, cos(\theta) + i_b\, cos(\theta - \frac{2\pi}{3}) + i_c\, cos(\theta + \frac{2\pi}{3})\right] \\ i_q &= -\frac{2}{3}\left[i_a\, sin(\theta) + i_b\, sin(\theta - \frac{2\pi}{3}) + i_c\, sin(\theta + \frac{2\pi}{3})\right] \end{aligned} \tag{2.33}$$

The last term of Equation 2.30 is the derivative form of the currents shown in Equation 2.33:

$$\begin{aligned}\frac{di_d}{dt} &= \frac{2}{3}\left[\frac{di_a}{dt}\,cos(\theta) + \frac{di_b}{dt}\,cos(\theta - \frac{2\pi}{3}) + \frac{di_c}{dt}\,cos(\theta + \frac{2\pi}{3})\right] \\ &\quad - \frac{2}{3}w\left[i_a\,sin(\theta) + i_b\,sin(\theta - \frac{2\pi}{3}) + i_c\,sin(\theta + \frac{2\pi}{3})\right] \\ \frac{di_q}{dt} &= -\frac{2}{3}\left[\frac{di_a}{dt}\,sin(\theta) + \frac{di_b}{dt}\,sin(\theta - \frac{2\pi}{3}) + \frac{di_c}{dt}\,sin(\theta + \frac{2\pi}{3})\right] \\ &\quad + \frac{2}{3}w\left[i_a\,cos(\theta) + i_b\,cos(\theta - \frac{2\pi}{3}) + i_c\,cos(\theta + \frac{2\pi}{3})\right]\end{aligned} \tag{2.34}$$

Using Equations 2.30, 2.31, 2.32, and 2.33, the new formulation of the KVL equation in the dq rotating frame is:

$$\begin{bmatrix}V_d^{grid}\\ V_q^{grid}\end{bmatrix} - \begin{bmatrix}V_d^{conv}\\ V_q^{conv}\end{bmatrix} = R\begin{bmatrix}i_d\\ i_q\end{bmatrix} + L\frac{d}{dt}\begin{bmatrix}i_d\\ i_q\end{bmatrix} + wL\begin{bmatrix}0 & -1\\ 1 & 0\end{bmatrix}\begin{bmatrix}i_d\\ i_q\end{bmatrix} \tag{2.35}$$

$$\begin{aligned}L\frac{di_d}{dt} &= -Ri_d + wLi_q + V_d^{grid} - V_d^{conv} \\ L\frac{di_q}{dt} &= -Ri_q - wLi_d + V_q^{grid} - V_q^{conv}\end{aligned} \tag{2.36}$$

where w is the AC angular frequency at the grid side.

The apparent power at the grid side is represented in the dq frame as follows:

$$\begin{aligned}S_{dq} &= \frac{3}{2}V_{dq}^{grid}i_{dq}^{*} \\ &= \frac{3}{2}(V_d^{grid} + jV_q^{grid})(i_d - ji_q) \\ &= \frac{3}{2}\left[\left(V_d^{grid}i_d + V_q^{grid}i_q\right) + j\left(V_q^{grid}i_d - V_d^{grid}i_q\right)\right]\end{aligned} \tag{2.37}$$

The active power of the grid input has an equal relationship with the DC output as expressed below:

$$\begin{aligned}P_{dq}^{grid} &= P_{dc} \\ \frac{3}{2}(V_di_d + V_qi_q) &= V_{dc}I_{dc}\end{aligned} \tag{2.38}$$

where

$$I_{dc} = C\frac{dV_{dc}}{dt} + I_L \tag{2.39}$$

The dq rotating frame has the d-axis aligned with the AC grid voltage phasor, using a Phase Locked Loop (PLL), which results in:

$$\begin{aligned} V_d &= V_{grid} \\ V_q &= 0 \end{aligned} \tag{2.40}$$

Hence, the active and reactive power from Equation 2.37 is:

$$\begin{aligned} P &= \frac{3}{2}V_d i_d \\ Q &= -\frac{3}{2}V_d i_q \end{aligned} \tag{2.41}$$

As can be seen in Equation 2.41, two parts of the currents in the d and q axes have been defined based on the transformation to the dq frame system. This implies the ability to independently control active and reactive power where i_d manages the amount of active power that is required from the system, whereas i_q regulates the levels of reactive power.

The angle θ, as previously mentioned, is needed for the transformation between the α-β and dq frames. This angle is located between the d-axis of the dq rotating frame and the α-axis of the α-β stationary frame, and is also known as the angular position of the voltage vector.

$$\theta = tan^{-1}\left(\frac{V_\beta}{V_\alpha}\right) \tag{2.42}$$

where V_α and V_β represent the voltage coordinates in α-β frame system. The value of the angle is determined by a PLL, which is a circuit used to synchronize a local voltage-controlled oscillator (VSO) with an input signal, and which also guarantees this VSO to have the same frequency and be in phase with the input. A PLL is not required in the case of connecting the VSC-HVDC to a passive grid since there is no synchronization issue

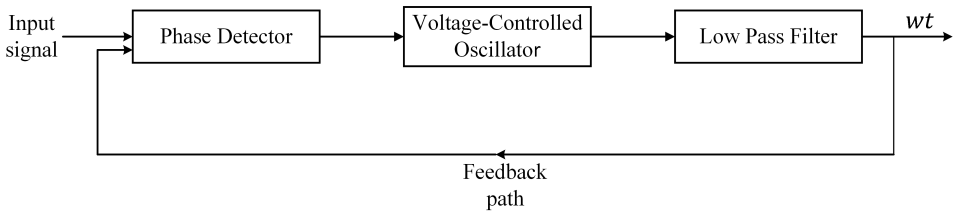

Figure 2.9: The main components of a PLL

if only one AC source exists in the system. In contrast, connecting an active AC grid to a VSC-HVDC station demands a frequency and phase synchronization at the point of common coupling (PCC). The main components of a PLL are shown in Figure 2.9.

A decoupled control of active and reactive power, which is one of the major advantages of vector control, requires a cascade control scheme. This control includes inner, outer, and PI controllers in which the inner current control is the output of the outer controllers. These outer controllers consist of DC voltage control, active power control, AC voltage control, and reactive power control. The active current has a reference value that is governed by the DC voltage and active power controllers. However, the reference reactive current is set by the AC voltage and reactive power controllers.

2.4.3 The Inner Current Controller

The operation and layout of the inner current control for the VSC station is shown in Figure 2.10 and based on the relationships in Equation 2.36 [26–29]. This equation contains cross-coupling and nonlinear terms that need to be eliminated in order to prevent any possible disturbance in the control system. As a result, a feed forward term in the controller loop is implemented to cancel the coupling effect caused by the inductance. The presence of PI controllers in the loop is essential in order to eliminate the dominant poles of the

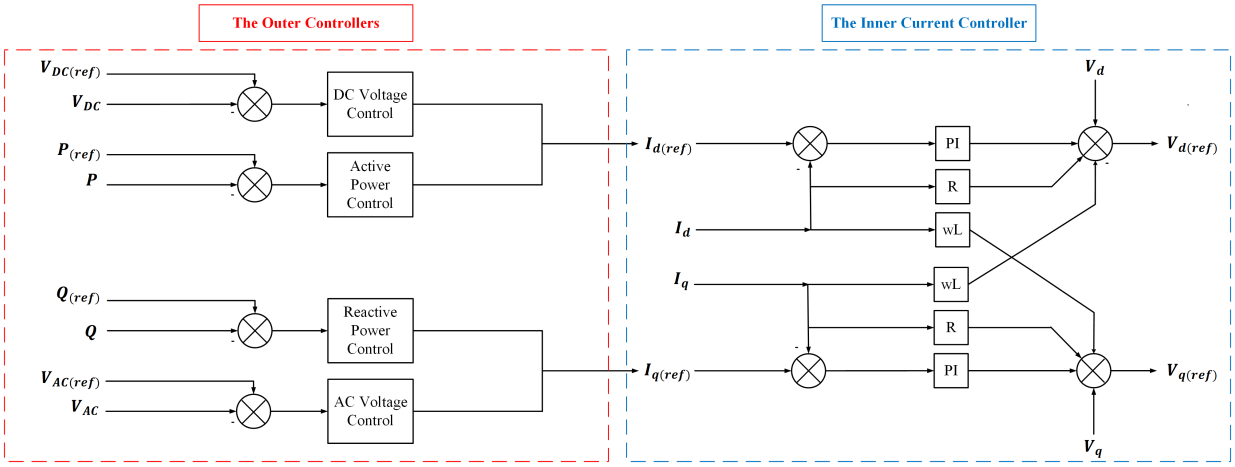

Figure 2.10: The inner and outer controllers

VSC by the zeroes of the PI controllers. After rearranging the terms of Equation 2.36:

$$\begin{aligned} V_d^{grid} - V_d^{conv} &= L\frac{di_d}{dt} + Ri_d - wLi_q \\ V_q^{grid} - V_q^{conv} &= L\frac{di_q}{dt} + Ri_q + wLi_d \end{aligned} \tag{2.43}$$

The two main equations of the PI controllers are:

$$\begin{aligned} P(s) = K_{pi} + \frac{K_c}{s} &= K_{pi}\left[\frac{1 + T_c \cdot s}{T_c \cdot s}\right] \\ T_c &= \frac{K_{pi}}{K_c} \end{aligned} \tag{2.44}$$

where K_{pi} is the proportional gain and T_c is the integral time constant, and the reference output voltage of the PI controller is:

$$V_{ref}^{conv}(s) = [I_{ref}(s) - I(s)]\left(K_{pi} + \frac{K_c}{s}\right) \tag{2.45}$$

Since the converter is considered to be an ideal transformer that has a time delay, the output voltage can expressed as:

$$V^{conv}(s) = V_{ref}^{conv}(s)\frac{1}{1 + T_d \cdot s} \tag{2.46}$$

where T_d is the time delay, which equals half of the switching time.

By substituting Equation 2.45 in Equation 2.46:

$$V^{conv}(s) = \left\{ [I_{ref}(s) - I(s)] \left(K_{pi} + \frac{K_c}{s} \right) \right\} \frac{1}{1 + T_d \cdot s} \tag{2.47}$$

By implementing Equation 2.47, the currents i_d and i_q have separate inner current controllers that lead to two reference values for the voltage:

$$\begin{aligned} V_d^{conv} &= (i_d^{ref} - i_d) \left(K_{pi} + \frac{K_c}{s} \right) \frac{1}{1 + T_d \cdot s} \\ V_q^{conv} &= (i_q^{ref} - i_q) \left(K_{pi} + \frac{K_c}{s} \right) \frac{1}{1 + T_d \cdot s} \end{aligned} \tag{2.48}$$

With the use of separate controllers, the currents in Equation 2.43 are not independent because they are controlled by the disturbance of cross-coupling inductance from wLi_q, wLi_d, and the grid's voltages V_d^{grid} and V_q^{grid}, as well as the effect of the converters' voltages V_d^{conv} and V_q^{conv}. Consequently, a negative feedback control and grid voltages feed-forward terms are necessary to attain an improved control and overall performance [30].

$$\begin{aligned} V_d^{conv*} &= -(i_d^{ref} - i_d) \left(K_{pi} + \frac{K_c}{s} \right) + wLi_q + V_d^{grid} \\ V_q^{conv*} &= -(i_q^{ref} - i_q) \left(K_{pi} + \frac{K_c}{s} \right) - wLi_d + V_q^{grid} \end{aligned} \tag{2.49}$$

Using Equations 2.43, 2.46, and 2.49, the two axes' currents i_d and i_q can be independently controlled by the addition of feed-forward compensations, which is the main feature of vector control.

$$\begin{aligned} V_d^{conv} &= L\frac{di_d}{dt} + Ri_d \\ V_q^{conv} &= L\frac{di_q}{dt} + Ri_q \end{aligned} \tag{2.50}$$

By applying Laplace transformation:

$$\begin{aligned} s \cdot i_d(s) &= -\frac{R}{L} \cdot i_d(s) + \frac{1}{L} V_d^{conv} \\ s \cdot i_q(s) &= -\frac{R}{L} \cdot i_q(s) + \frac{1}{L} V_q^{conv} \end{aligned} \tag{2.51}$$

Resulting in

$$\begin{aligned} i_d(s) &= \frac{1}{s \cdot L + R} \cdot V_d^{conv} \\ i_q(s) &= \frac{1}{s \cdot L + R} \cdot V_q^{conv} \end{aligned} \tag{2.52}$$

Therefore, the system transfer function is:

$$T(s) = \frac{1}{R\left(1 + s \cdot \frac{L}{R}\right)} = \frac{1}{R} \cdot \frac{1}{1 + s \cdot \tau} \tag{2.53}$$

Transforming this equation to per unit representation has to begin with Equation 2.51:

$$L \cdot s \cdot i_d^{pu}(s) \cdot I_b + R \cdot i_d^{pu}(s) \cdot I_b = V_d^{conv,pu} \cdot V_b \tag{2.54}$$

$$L \cdot s \cdot i_d^{pu}(s) \cdot \frac{I_b}{V_b} + R \cdot i_d^{pu}(s) \cdot \frac{I_b}{V_b} = V_d^{conv,pu} \tag{2.55}$$

$$\frac{L_{pu}}{w_b} \cdot s \cdot i_d^{pu}(s) + R_{pu} \cdot i_d^{pu}(s) = V_d^{conv,pu} \tag{2.56}$$

$$\frac{L}{w_b} \cdot s \cdot i_d^{pu}(s) + R_{pu} \cdot i_d^{pu}(s) = V_d^{conv,pu} \tag{2.57}$$

$$\frac{i_d^{pu}(s)}{V_d^{conv,pu}} = \frac{1}{R_{pu}} \cdot \frac{1}{1 + \left(\frac{L_{pu}}{w_b R_{pu}}\right) \cdot s} \tag{2.58}$$

Thus, the per unit transfer function of the system is:

$$\frac{i_d^{pu}(s)}{V_d^{conv,pu}} = \frac{1}{R_{pu}} \cdot \frac{1}{1 + \tau_{pu} \cdot s} \tag{2.59}$$

PI controllers in a VSC-HVDC follow the same process as electric drives in terms of the tuning operation. These controllers must be tuned in order to achieve the best possible optimal operation outcome by increasing the response speed of the system. The modulus optimum method is used to tune the PI controllers in the inner control loop. When the transfer function has one dominant pole and second minor pole, the modulus optimum technique is performed by eliminating the dominant pole using the controller zero which is

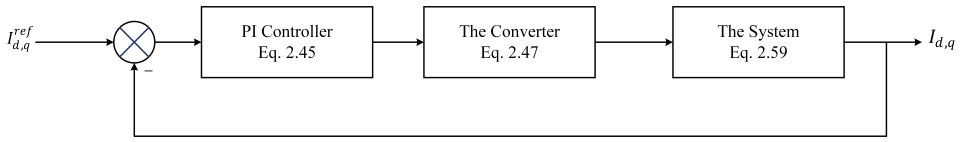

Figure 2.11: A flowchart of the inner controller

the integral time constant in this case. Based on Equations 2.45, 2.47, and 2.59 as shown in Figure 2.11, the formulation of the open loop transfer function of the controller is:

$$T_{O.L.}(s) = \left(K_{pi}^{pu} \cdot \frac{1 + T_c \cdot s}{T_c \cdot s}\right) \cdot \left(\frac{1}{1 + T_d \cdot s}\right) \cdot \left(\frac{1}{R_p u} \cdot \frac{1}{1 + s \cdot \tau_{pu}}\right) \tag{2.60}$$

The dominant pole of the transfer function is cancelled by the zero of the controller due to the use of the modulus optimum technique, and the time constant T_c is defined as τ_{pu}.

$$T_{O.L.}(s) = \frac{K_p^{pu}}{\tau_{pu} \cdot R_{pu}} \cdot \frac{1}{s \cdot (1 + T_d \cdot s)} \tag{2.61}$$

By applying the unity gain condition, the proportional gain of the controller is:

$$|T_{O.L.}(s)| = \left|\frac{K_p^{pu}}{\tau_{pu} \cdot R_{pu}} \cdot \frac{1}{s \cdot (1 + T_d \cdot s)}\right| \tag{2.62}$$

$$K_{pi} = w_{co} \tau R_{pu} (1 + T_c^2 w_{co}^2)^{\frac{1}{2}} \tag{2.63}$$

where w_{co} is the cutoff frequency. The time constant is:

$$T_c = \tau_{pu} \tag{2.64}$$

From Equation 2.61, the closed loop transfer function can be written as:

$$T_{C.L.}(s) = \frac{1}{2T_d^2 \cdot s^2 + 2T_d \cdot s + 1} \tag{2.65}$$

2.4.4 The Outer Controllers

The outer controllers in the VSC include active power control, reactive power control, AC voltage control at the PCC, and DC voltage at the DC bus, as illustrated in Figure 2.10. The active current i_d is implemented to control the active power flow and DC voltage level, whereas the reactive current i_q regulates the reactive power and AC voltage.

Active and reactive power control loops in the outer control controllers are represented and based on Equation 2.40 and Equation 2.41 [26, 27]. PI controllers are used in both loops in order to reach a better control in which the i_d^{ref} is the output of the active power controller, and i_q^{ref} is the reactive power's output based on the scope of this thesis, as shown in Figure 2.10. These outputs have limits in order to control the current in the VSC station where i_d^{ref} is limited by $\pm i_{max}$, and i_q^{ref} is limited by $\pm i_{q_{max}}$ as well as the condition that the rated current is less than the VSC current.

$$\begin{aligned} i_{rated} &= i_{max} \\ i_q^{ref} &= \sqrt{(i_{max})^2 - (i_d^{ref})^2} \end{aligned} \tag{2.66}$$

The DC voltage controller principle is based on the power balance equation of the VSC station:

$$\begin{aligned} P_{ac} + P_{dc} + P_{cap} &= 0 \\ \frac{3}{2} V_d i_d + V_{dc} I_{dc} + V_{dc} i_{cap} &= 0 \end{aligned} \tag{2.67}$$

where I_{dc} is the current at the DC bus, and i_{cap} is the current flowing through the capacitor which can be expressed from the same equation by:

$$i_{cap} = -\left(\frac{3V_d i_d}{2V_{dc}} + I_{dc}\right) \tag{2.68}$$

This capacitor current can also be represented based on the voltage across the capacitor by:

$$i_{cap} = C\frac{dV_{dc}}{dt} \tag{2.69}$$

Combining Equation 2.68 and Equation 2.69 gives the differential equation of the DC voltage:

$$\frac{dV_{dc}}{dt} = -\frac{3V_d i_d}{2CV_{dc}}\left(i_d + \frac{2V_{dc}I_{dc}}{3V_d}\right) \tag{2.70}$$

From Equation 2.70, the I_{dc} term is replaced by a feed-forward in the DC voltage controller, which is completely regulated by the active current i_d.

The PI equations in the DC voltage outer controller are given as follows:

$$\begin{aligned} P(s) = K_{pi} + \frac{K_v}{s} &= K_{pi}\left[\frac{1 + T_v \cdot s}{T_v \cdot s}\right] \\ T_v &= \frac{K_{pi}}{K_v} \end{aligned} \tag{2.71}$$

where K_{pi}, K_v, and T_v are the voltage parameters of the PI controllers.

$$i_{dc}^{ref}(s) = \left[V_{dc}^{ref}(s) - V_{dc}(s)\right]\left(K_{pi} + \frac{K_v}{s}\right) \tag{2.72}$$

From Equation 2.38 and Equation 2.40, the I_{dc} equation in terms of the active current is:

$$I_{dc} = \frac{3}{2} \cdot \frac{v_d}{V_{dc}} \cdot i_d \tag{2.73}$$

Using Equation 2.39:

$$C\frac{dV_{dc}}{dt} = \frac{3}{2} \cdot \frac{v_d}{V_{dc}} \cdot i_d - I_L \tag{2.74}$$

Equation 2.74 is a nonlinear equation that requires linearization using a Taylor series. This expansion depends on one variable, which is the reference voltage input V_{dc}^{ref}, and by multiple condition points x_0, y_0, and z_0:

$$\begin{aligned} \frac{dx}{dt} &= f(x, y, z) \\ \frac{d\Delta x}{dt} &= \frac{\partial f}{\partial x}\Big|_{\substack{y=y_0 \\ z=z_0}} \cdot \Delta x + \frac{\partial f}{\partial y}\Big|_{\substack{x=x_0 \\ z=z_0}} \cdot \Delta y + \frac{\partial f}{\partial z}\Big|_{\substack{x=x_0 \\ y=y_0}} \cdot \Delta z \\ C\frac{dV_{dc}}{dt} &= \frac{3}{2} \cdot \frac{v_{d0}}{V_{dc}^{ref}} \cdot \Delta i_d + \frac{3}{2} \cdot \frac{i_{d0}}{V_{dc}^{ref}} \cdot \Delta v_d - \left(\frac{3}{2} \cdot \frac{v_{d0} \cdot i_{d0}}{V_{dc}^{2ref}}\right) \cdot \Delta V_{dc} - \Delta I_L \end{aligned} \tag{2.75}$$

Since the main focus in this controller is i_d, the linearization equation is:

$$\frac{d\Delta V_{dc}}{dt} = \frac{3}{2} \cdot \frac{v_{d0}}{V_{dc}^{ref}} \cdot \Delta i_d \tag{2.76}$$

By applying Laplace transformation:

$$\frac{\Delta V_{dc}(s)}{\Delta i_d(s)} = \frac{3}{2} \cdot \frac{v_{d0}}{V_{dc}^{ref}} \cdot \frac{1}{s \cdot C} \tag{2.77}$$

The DC voltage controller aims to achievie power balance conditions by regulating the capacitor current i_c. In other words, i_c equals zero when the conditions are fulfilled; therefore, I_L=I_{dc} and the feed-forward term is:

$$i_d = \frac{2}{3} \cdot \frac{V_{dc}}{v_d} \cdot I_L \tag{2.78}$$

The per unit representation of the power balance equation in Equation 2.73 and its expression as a power invariant are, respectively:

$$\begin{aligned} I_{dc}^{pu} \cdot I_{dc}^{base} &= \frac{3}{2} \cdot \frac{v_d^{pu} \cdot V_b}{V_{dc}^{pu} \cdot V_{dc}^{base}} \cdot i_d^{pu} \cdot I_b \\ I_{dc}^{pu} &= \frac{v_d^{pu}}{V_{dc}^{pu}} \cdot i_d^{pu} \end{aligned} \tag{2.79}$$

Expressing Equation 2.69 in per unit, then using Laplace transformation, is depicted, respectively, as:

$$\begin{aligned} \frac{1}{w_b \cdot C_{pu}} \cdot \frac{dV_{dc}^{pu}}{dt} &= I_{dc}^{pu} - I_L^{pu} \\ V_{dc}^{pu}(s) &= \frac{w_b \cdot C_{pu}}{s} \left(I_{dc}^{pu}(s) - I_L^{pu}(s)\right) \end{aligned} \tag{2.80}$$

The feed-forward Equation 2.78 in per unit is:

$$i_d^{pu} = \frac{V_{dc}^{pu}}{v_d^{pu}} \cdot I_L^{pu} \tag{2.81}$$

The PI controller is tuned based on the modulus optimum technique when the open transfer function has a dominant and a minor pole. In contrast, when the open transfer

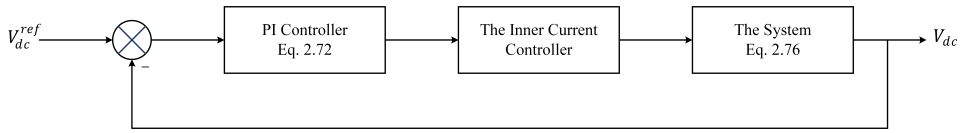

Figure 2.12: A flowchart of the outer controller

function has a pole near or at the origin, the symmetrical optimum technique is implemented instead of the modulus optimum. The symmetrical optimum technique can be defined as an optimization approach in which a controller demands the frequency response to be within the range of low frequency systems. The main advantage of the symmetrical optimum over other methods is its ability to maximize the phase margin. This feature is necessary for systems where delays and disturbances are frequent.

The open loop transfer function of the system is presented in a per unit expression as well as in terms of PI controllers, the inner current controller, and the system dynamics, as illustrated in Figure 2.12.

$$T_{O.L.}(s) = \left(K_{pi}^{pu} \cdot \frac{1 + T_v \cdot s}{T_v \cdot s}\right) \cdot \left(\frac{1}{1 + T_{eq} \cdot s}\right) \cdot \left(\frac{v_d^{pu}}{V_{dc}^{pu}} \cdot \frac{w_b \cdot C_{pu}}{s}\right) \tag{2.82}$$

in which:

$$T_{eq} = 2T_d \tag{2.83}$$

$$\begin{aligned} \angle T_{O.L.}(s) &= -180^\circ + tan^{-1}(wT_v) - tan^{-1}(wT_{eq}) \\ \angle T_{O.L.}(s) &= -180^\circ + \phi_m \end{aligned} \tag{2.84}$$

where ϕ_m is the phase margin that its maximum value can be obtained when ϕ_m is differentiated with respect to w, and equated to zero.

$$\frac{d\phi_m}{dw} = \frac{T_v}{1 + (wT_v)^2} - \frac{T_{eq}}{1 + (wT_{eq})^2} = 0, \text{ when } w = \frac{1}{\sqrt{T_v T_{eq}}} \tag{2.85}$$

As a result, the angle of the phase margin is:

$$\angle\phi_m = tan^{-1}\sqrt{\frac{T_v}{T_{eq}}} - tan^{-1}\sqrt{\frac{T_{eq}}{T_v}} \tag{2.86}$$

when the first term of the previous equation is assumed to be:

$$tan^{-1}\sqrt{\frac{T_v}{T_{eq}}} = \vartheta \tag{2.87}$$

Consequently, Equation 2.86 can be written as:

$$\angle\phi_m = \vartheta - (90 - \vartheta) \tag{2.88}$$

Using Equations 2.86, 2.87, and 2.88, the time constant of the controller is expressed as:

$$T_v = T_{eq} \cdot \left[\frac{1 + sin\phi_m}{1 - sin\phi_m}\right] \tag{2.89}$$

The proportional gain is determined based on the unity gain condition.

$$|T_{O.L.}(s)| = \left|\left(K_{pi}^{pu} \cdot \frac{1 + T_v \cdot s}{T_v \cdot s}\right) \cdot \left(\frac{1}{1 + T_{eq} \cdot s}\right) \cdot \left(\frac{v_d^{pu}}{V_{dc}^{pu}} \cdot \frac{w_b \cdot C_{pu}}{s}\right)\right| = 1 \tag{2.90}$$

$$K_{pi}^{pu} = \frac{\frac{1}{w_b \cdot C_{pu}}}{\frac{v_d}{V_{dc}} \cdot \sqrt{T_v \cdot T_{eq}}} \tag{2.91}$$

The closed loop transfer function of the DC voltage controller is:

$$T_{C.L.}(s) = \frac{1 + a^2 \cdot T_{eq} \cdot s}{1 + a^2 \cdot T_{eq} \cdot s + a^3 \cdot T_{eq}^2 \cdot s^2 + a^3 \cdot T_{eq}^3 \cdot s^3} \tag{2.92}$$

where a is the distance between $1/T_v$ to w, and from w to $1/T_{eq}$.

The AC voltage controller depends on the KVL equation across the line reactor:

$$\begin{aligned} V_{grid}^{ref} - V_{conv} &= X \cdot i_{conv} \\ V_{grid}^{ref} &= V_{conv} + (r + jwl)\left(\frac{P - jQ}{V_{grid}^{ref}}\right) \\ V_{grid}^{ref} &= V_{conv} + \left(\frac{Pr + Qwl}{V_{grid}^{ref}}\right) + j\left(\frac{Pwl - Qr}{V_{grid}^{ref}}\right) \end{aligned} \tag{2.93}$$

As can be seen in Equation 2.93, the imaginary part of the equation has a minor impact on V_{grid}^{ref}, and ($wl \gg r$) in most AC systems; therefore, V_{grid}^{ref} is only dependable on the flow of reactive power.

$$V_{grid}^{ref} = \frac{wl}{V_{grid}^{ref}} Q \tag{2.94}$$

The operation of the AC voltage controller can be summarized based on Equation 2.41 and Equation 2.94.

2.5 VSC-HVDC Configurations

The implementation of VSC-HVDC connections of two or more terminals has growing applications, such as interconnecting between renewable energy sources and AC systems, and transmitting power from or to offshore areas, which results in a number of various structures for HVDC systems. These arrangements differ in converters locations, lines, and advantages, based on function and cost.

2.5.1 A Monopolar HVDC system

This configuration has two main types, as listed below:

1. An Asymmetric Monopole

   An asymmetric monopole connection is a single conductor that separates two converters with either a positive or negative DC voltage, as shown in Figure 2.13. The return current in this configuration can use the ground or a metallic return conductor as a path.

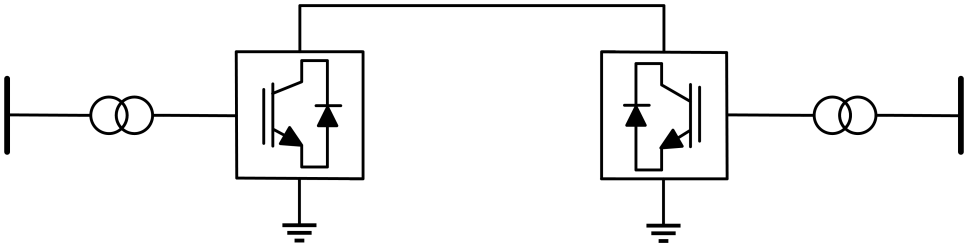

Figure 2.13: An asymmetric monopole HVDC system

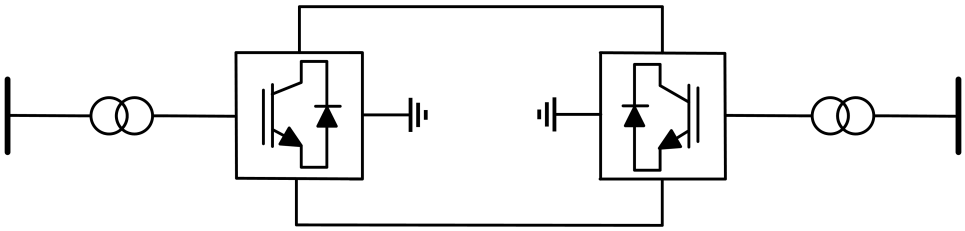

Figure 2.14: A symmetric monopole HVDC system

2. A Symmetric Monopole

   A symmetric monopole has two conductors with opposite DC voltage polarity, and a mid-point ground at the DC side that has no flowing current during normal conditions as demonstrated in Figure 2.14. In the case of a fault between the one of the conductors and the ground, the DC side will receive no current from the AC side.

2.5.2 A Bipolar HVDC system

The bipolar connection has four converters, and two insulated conductors with a different voltage polarity, as illustrated in Figure 2.15. Both these two poles can be grounded, which allows them to work independently. This means that both poles have equal current with no ground current under normal operation whereas, in abnormal conditions, one of the poles can operate its two converters solely and use the ground as a path. Thus, the reliability of

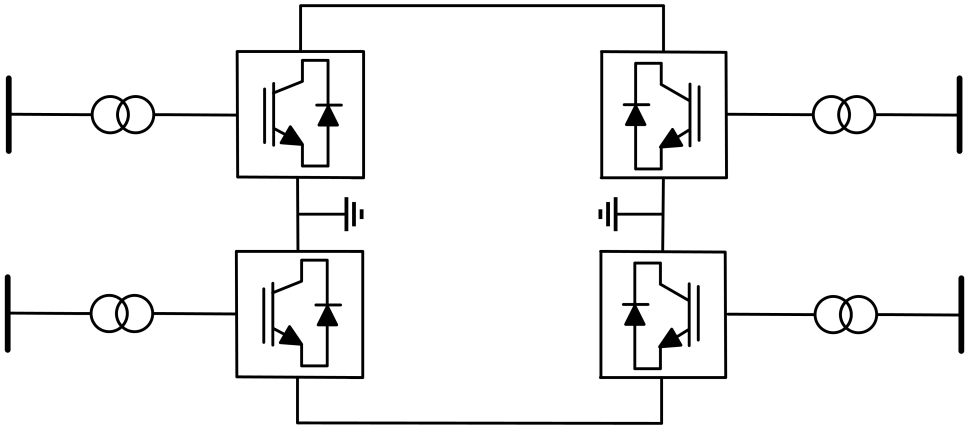

Figure 2.15: A bipolar HVDC system

this configuration is higher, but it is not cost-effective.

2.5.3 A Multi-Terminal HVDC System

This arrangement has more than two converters that are separated by long transmission lines and placed over a large geographical area. The primary aim of this type is to provide more reliability as well as being cost and operation efficient.

2.6 Per-Unit Representation

A per-unit system is needed to simplify the design and use of different controllers in VSC-HVDC systems. This system is based on the peak values of voltage and current as well as the power rating. In VSC-based systems, the p.u. conversation in the dq frame is categorized into two parts based on the sides of the VSC station: AC and DC terms, as shown in Table 2.1.

Table 2.1: P.U. quantities

AC side	
Power	$\mathrm{S}_{base} = 3 \cdot V_{rms} \cdot I_{rms} = \frac{2}{3} \cdot V_{peak} \cdot I_{peak}$
Voltage	$\mathrm{V}_{base,ac} = \sqrt{\frac{2}{3}} \cdot V_{LL,rms}$
Current	$\mathrm{I}_{base,ac} = \frac{S_{base}}{V_{base}}$
Resistance	$\mathrm{R}_{base,ac} = Z_{base,ac} = \frac{V_{base}}{I_{base}}$
Capacitance	$\mathrm{C}_{base} = \frac{1}{Z_{base,ac} \cdot w_{base}}$
Inductance	$\mathrm{L}_{base} = \frac{Z_{base,ac}}{w_{base}}$
Frequency	ω_b
DC side	
Voltage	$\mathrm{V}_{base} = 2 \cdot V_{base,ac}$
Current	$\mathrm{I}_{base} = \frac{S_{base}}{V_{base,dc}}$
Resistance	$\mathrm{R}_{base,dc} = Z_{base,dc} \frac{V_{base,dc}}{I_{base,dc}}$

Chapter 3

Power Sharing Control in MTDC VSC-based Systems and the Proposed Control Strategy[1]

One of the major applications of MTDC systems is to integrate renewable energy sources, such as offshore wind farms, into onshore AC grids as well as implemented in distribution systems, which results in a wide range of possible benefits. MTDC systems in these types of applications transmit power from the generation stage to AC grids at the end side in order to guarantee a suitable power sharing among different stations that are connected to the MTDC system. Achieving a desired power sharing level is considered to be a significant challenge in MTDC systems due to the complexity of the system and device

[1] A part of this section has been published in:
Khaled Alshammari, Hasan Alrajhi Alsiraji, and Ramadan El Shatshat. Optimal Power Flow in Multi-Terminal HVDC Systems. *2018 IEEE Electrical Power and Energy Conference, EPEC 2018*, pages 1-6, 2018

level issues. From the system level, the process of power sharing among MTDC stations must be performed under the conditions of a balanced power, while maintaining the DC voltage level within acceptable limits in order to operate a stable system. At the device level, power sharing methods provide converters with predefined or fixed values that have to be satisfied, which may cause overloading in some parts of the system.

Power sharing schemes are used in MTDC systems to fulfil certain objectives such as minimizing transmission line losses, prioritizing specific converters, and varying the amount of power sharing.

Although many methods have been implemented to operate and control power sharing among MTDC terminals, the main and most commonly used techniques can be classified into five types. These five types are described in Sections 3.1-3.5 below.

3.1 Master-Slave Control

In this technique, the DC voltage regulation across the system is the task of one centralized converter, known as the master converter. This converter operates in constant voltage mode, whereas the other converters, named slave converters, work in constant power mode. The outer control loop of the master converter regulates the DC voltage level, and the other converters govern the power flow in the system. These constant-power converters receive their power reference values from the master converter using OPF calculations, while the master converter has a reference DC voltage value that must be within system constraints [31–34]. The major drawbacks of implementing the master-slave method include the need for fast communication and reliability since this method adopts a centralized scheme and fast communication is required between the master and slave converters to reach a proper power balance and sharing. This method cannot be used in a large-scale system due to the

presence of one voltage-regulating converter. In order to overcome any possible outages or over-limit cases, the master converter should operate with high rated power which causes an increase in cost and losses.

3.2 Voltage Margin Control

The voltage margin voltage technique is an alternative master-slave control in which the master converter can be replaced by multiple converters to control the DC voltage in the system. In normal operations, the master converter regulates the DC voltage, while the remaining converters work in constant power mode. However, the other converters, which are back-up converters, start to regulate the DC voltage in the case of a master converter failure and operate within local voltages and power ratings [35]. The operation of voltage margin control can be explained as the master converter maintains the DC voltage level at a certain voltage point (V_1) but, in the case of an outage, the DC voltage either rises or drops. When the DC voltage rises, the terminal with a higher reference voltage point (V_2) stops working in constant power mode and starts to govern the DC voltage across the system as shown in Figure 3.1. In the case of a voltage drop, the station with the lower voltage reference acts as the DC voltage regulator. Therefore, this technique can be operated without the need for communication among terminals regarding the use of predefined voltage and power reference values [36]. Hence, the difference between voltage references of the master converter and other backup converters is the voltage margin, as shown in Equation 3.1:

$$\Delta V_{margin} = V_{master}^{ref} - V_{backup}^{ref} \tag{3.1}$$

In a two-stage voltage margin control, voltage and power-controlled converters are operated based on upper and lower power limits in order to transfer power within the system.

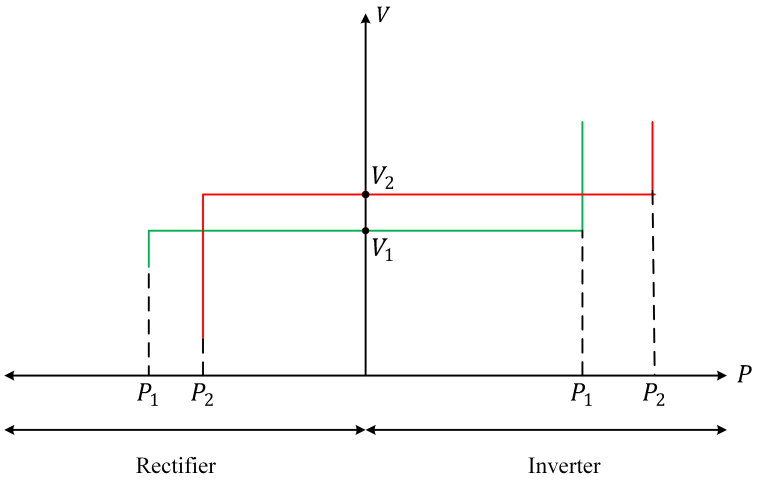

Figure 3.1: Voltage margin control

The maximum DC current sets these limits while taking power flow conditions into consideration. This scheme has the edge over one-stage margin voltage control in terms of using one backup converter that can act as master converter in a voltage rise and drop cases.

This method has a number of disadvantages, such as the issue that only fixed power sharing is implemented and transient response is slow due to the presence of multiple control loops. Using more voltage and power references provides more flexibility to the system; nevertheless, this causes more complexity in terms of the method dynamics.

3.3 Droop Control

The voltage droop control is considered to be the DC alternative of power-frequency droop control in AC systems where the frequency is generally the indication of a stable AC grid. The same applies to DC voltage in DC grids. Specifically, any rise or drop in frequency is driven by load changes on the consumer side. Similarly, the DC voltage level in an MTDC

system is triggered by a power increase or decrease that requires the VSC stations to balance the difference by adjusting their current. The power flow between the terminals of the MTDC system is mainly affected by the voltage level throughout the grid. Therefore, the voltage droop control regulates the DC voltage among the terminals under the condition of achieving power balance in the entire system. Using a decentralized approach, droop control allows two or more converters to regulate the DC voltage based on specific droop characteristics, while the remainder of the converters work as constant power terminals [37].

Droop control improves the system reliability since all the droop terminals can regulate the DC voltage. This is a significant advantage especially when there is an outage in a station since the system remains in operation regardless of the outage. Low-rated power terminals are implemented for large power balances throughout the system since all droop stations share the voltage and power control. One the contrary, one of the main disadvantages of droop control is that the power sharing among the system terminals depends on the DC voltage differences which results in an unsuitable power flow. Therefore, the proposed control strategy in thesis applies a secondary control level to overcome the aforementioned drawback.

3.4 Priority Control

This method can be defined as a master-slave control with droop-controlled terminals or a combination of constant-voltage and droop control techniques. Priority control is so named since it gives priority to one station over other stations in terms of gaining power until the maximum predefined value is reached. In normal operations, the priority station operates in constant voltage mode, and regulates the DC voltage in the system. However, the other terminals work in constant power mode with droop control. In abnormal circumstances,

the high priority terminal, which may have an outage or may exceed the power limit, starts to work in constant power mode, which results in an increase in the DC voltage, causing the rest of the converters to work in droop control and to regulate the DC voltage. Specifically, the DC voltage reaches the minimum voltage limit of the second terminal, which is higher than the maximum voltage limit of the priority terminal, and the second station acts as the voltage regulator [38, 39].

Priority control requires high voltage rated terminals that work with droop control to operate without the need of communication. Therefore, the cost of all terminals, with the exception of the high priority terminal, is higher than other control techniques. Systems with many terminals cannot implement priority control due to the difficulty of the design and operation on a large scale. The approach of using designated stations may cause an inefficient use of the entire system capabilities.

3.5 Ratio Control

Ratio control is a droop control with a ratio between voltage-controlled terminals for the purpose of sharing all the generated power in the system [40]. This approach provides the ability to change the droop slope in order to control the power-sharing ratio among terminals that regulates the DC voltage, unlike the droop control method. In the case of an MTDC system with two VSCs at the grid side, the first terminal has fixed droop characteristics, whereas the second VSC has flexible droop characteristics in order to meet the conditions, as shown in Equation 3.2 [38]:

$$\begin{aligned} n &= \frac{P_1}{P_2} = \frac{R_2 + \frac{1}{k_2}}{R_1 + \frac{1}{k_1}} \\ k_2 &= \frac{1}{n \cdot (R_1 - R_2) + \frac{n}{k_1}} \end{aligned} \tag{3.2}$$

where n is the power ratio, R is the resistance of the DC cables, and k_1 and k_2 are the droop characteristics of VSC1 and VSC2. This equation shows that the power ratio between the two VSCs has to be the same value n.

Ratio control has several drawbacks, including the effect of the DC cables' resistance that may vary due to temperature, which causes imprecise power ratio. In addition, this method has a complex mathematical approach, especially with the calculation of a high number of power ratios within large systems.

3.6 VSC Station Losses

HVDC-based VSC systems are mainly employed in transmission stages of power systems due to the development of power electronics devices, and the ability to transfer power over long distances. Using a VSC station has numerous advantages, including the high and independent controllability of both active and reactive powers as well as the bidirectional power flow. In contrast, VSC stations carry several disadvantages, such as lower power capability compared to LCC. However, because of its effect on operational and power sharing efficiency, the most important disadvantage concerns the issue of losses. These losses can be defined as the sum of each component loss in the VSC station. The main components regarding losses are described in the following sections.

3.6.1 Transformer

Transformers are almost the same in AC and HVDC systems with the exception of harmonics caused by the VSC current. Losses in transformers are primarily divided into two types: load losses and no-load losses.

Load losses, also known as copper or winding losses, are the simplest form of losses whereby a higher current level and higher resistance lead to higher losses. These losses are mainly caused by several reasons such as the DC resistance of the windings, and the current carrying the harmonics through the windings. In contrast, no-load losses, namely core or iron losses, which are created by the variations in the flux, include two major kinds: eddy losses, which occur in the material of the core and hysteresis Losses, which refers to the power dissipated in the form of heat because of the change of magnetic field across the core. The presence of leakage of the magnetic flux results in a small amount of losses known as stray losses.

3.6.2 AC Filter

An AC filter, which is used to redirect the VSC harmonic current to the ground, consists of capacitance, inductance and resistance. The high-pass filter is the most common type in which the resistance and inductance are connected in parallel. The components of a high-pass filter play an important role in the number of losses. The capacitor losses are solely affected by its Equivalent Series Resistance (ESR), whereas the power losses of resistance are based on the square value of the current flowing through the resistance.

3.6.3 Phase Reactor

A phase reactor is designed to separate the AC frequency from the PWM signal, particularly to cancel the effect of high frequency disturbance using a series connection. This connection contains a reactance in series with a resistance, and the losses in the phase reactor are in the form of the dissipated power across the resistance.

3.6.4 Valves Consisting of IGBT's and Anti-Parallel Diodes

Valve losses represent the higher amount of losses in a VSC station, and switching and conduction losses are considered to be the main types.

3.6.5 DC Capacitor

Since DC capacitors lessen the effect of harmonics ripple, the losses in capacitors are mainly dependent on the harmonic current.

3.6.6 VSC Loss Model

A generalized loss model is presented, including all the main components of the VSC station, and used in the reminder of the thesis [41]. This model is also implemented in the load flow calculations, and in the control scheme technique. The data were based on the the Södra Länken HVDC Light® link, which was rated at 600 MW and a DC voltage of ± 300 kV, operating at a power factor of 1. The losses in this model can be categorized into constant terms, and dependent terms on the phase reactor current I_p, either linearly or quadratically. I_p is calculated based on the active and reactive power that is delivered or received by the converter, and the phase voltage.

$$I_p = \frac{\sqrt{P_c^2 + Q_c^2}}{\sqrt{3}V_c} \tag{3.3}$$

This current has an upper limit, which is:

$$|I_c| \leq I_c^{max} \tag{3.4}$$

Constant losses include transformer no-load losses, load losses, and filter losses, which are 0.36 MW, 1.26 MW, and 5 MW, respectively. Linear-dependent losses on the value of I_p

are represented by the equation:

$$P_{loss}^{linear} = 3 \times 600V \times I_p \tag{3.5}$$

Quadratic-dependent losses are divided based on the operation of the converter. Rectification or inversion, and the relationship of these losses, are described in:

$$\begin{aligned} P_{loss,rec}^{square} &= 3 \times 0.66\Omega \times I_p^2 \\ P_{loss,inv}^{square} &= 3 \times 1\Omega \times I_p^2 \end{aligned} \tag{3.6}$$

The overall losses of the converter under nominal conditions are 1.72% in case of a rectification mode, which is 10.34 MW based on the ratings of the aforementioned VSC. In contrast, the converter has 1.81% of losses when the VSC operates as an inverter, which results in 10.86 MW. Therefore, the VSC station losses are a function of the phase reactor current, and are represented by the following equation:

$$P_{loss}^{conv} = a + b \cdot I_p + c \cdot I_p^2 \tag{3.7}$$

where a,b, and c are positive coefficients in which a is the total transformer losses, b represents the linear-dependent losses, and c is the overall quadratic-dependent losses.

3.7 The Proposed Control Scheme

A hierarchical control scheme, which is shown in Figure 3.2, consists of an upper control and a lower control in order to achieve an optimal power-sharing control. The lower control level, which is the primary control, operates locally in each VSC station. In this thesis, the primary control is the DC voltage droop control. This control is responsible for both DC voltage levels and power balance across the system. The voltage-droop controlled

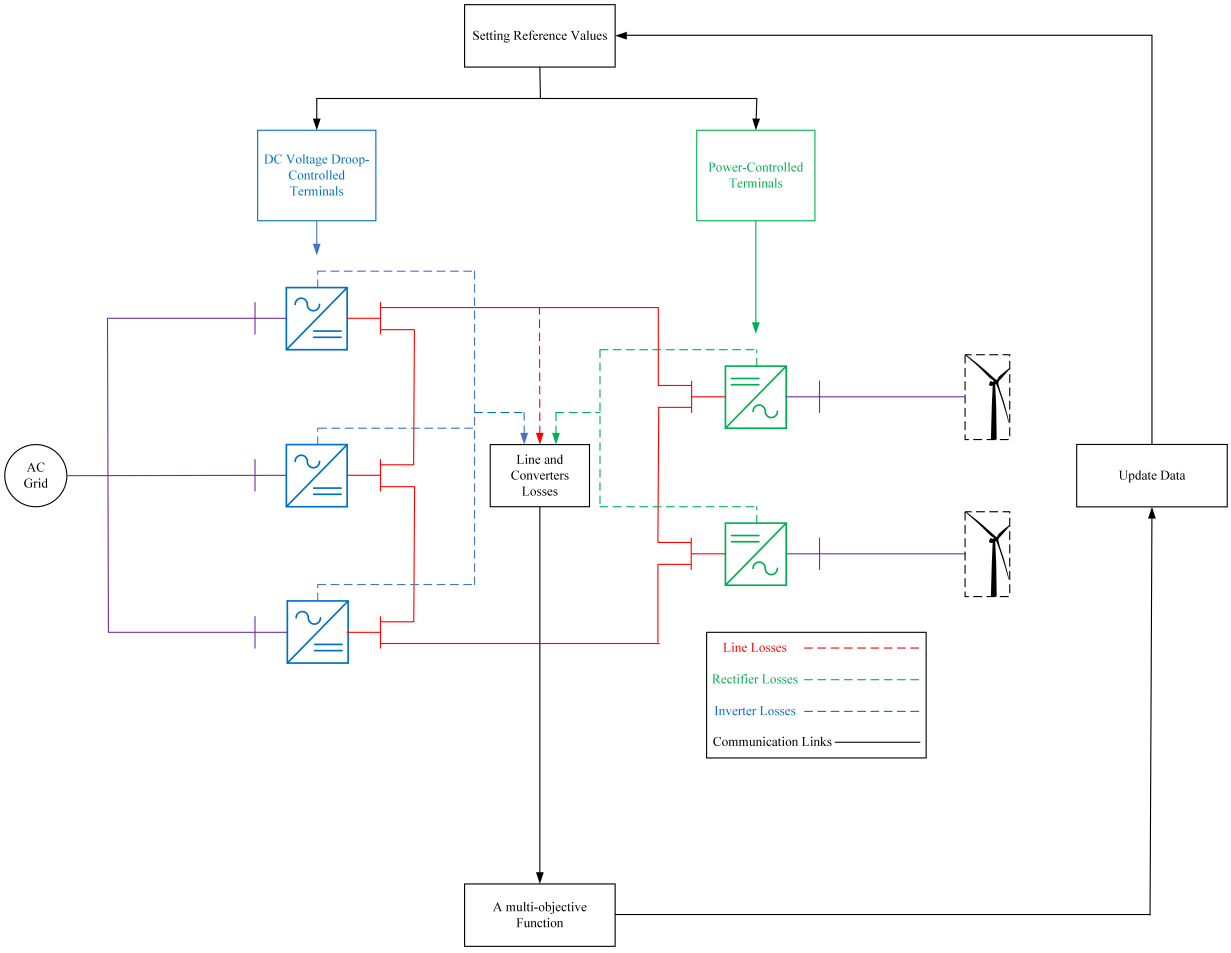

Figure 3.2: The proposed control scheme

terminals in the system share power based on predefined power shares. In the lower control, an optimization algorithm, namely, SDP, is implemented as a secondary control that operates globally to set the droop characteristics and voltage settings in order to meet a multi-objective function that enhances the accuracy of power sharing in the primary level. The OPF problem is solved using CVX, a package for specifying and solving convex programs [42, 43].

A generalized voltage droop control technique is presented in [44] for DC voltage control and power sharing in VSC-MTDC systems. This technique acts as the primary control in a two-layer hierarchical control system and operates in three different modes: conventional voltage droop control; fixed active power control; and fixed dc voltage control. In [45], the authors included dead-band in an enhanced DC voltage droop control method for MTDC systems. This method differs from previous DC voltage droop control techniques in which the VSC stations are categorized into four groups, where each group has its own voltage margin and dead-band. Therefore, the VSC stations can operate based on new power-voltage characteristics selected by the droop control method. A voltage droop control was implemented in [46] for VSC-HVDC transmission systems with offshore wind farms. The Lyapunov theory was used to set the converters parameters in order to optimize power sharing and stabilize the DC voltage of the system.

The authors in [47] presented a hierarchical control approach for MTDC where the primary controller is decentralized with a generalized voltage droop method, whereas the secondary control is a centralized controller with an OPF that has the transmission losses as its only parameter of the objective function. In addition, the secondary controller has to set the reference values of the primary without compromising the stability of the system. In order to achieve this, a central regulator is introduced with a closed loop integral control. In comparison, in [48], the hierarchical control of meshed MTDC systems was addressed by introducing a novel algorithm to solve the optimal power flow of DC systems. This algorithm is based on a distributed approach where the aim is to replace the conventional centralized secondary control of MTDC systems. Therefore, this approach induces each node in the system to solve its own objective function, and also to self-coordinate and corporate with the rest of the system. These steps are required in order to reach a global optimum operating point. In addition, the authors in [49] proposed a hierarchical control

to minimize the losses in a hybrid MTDC transmission system with wind farms. The optimal power flow control of a 6-terminal hybrid MTDC system consists of two layers, the first of which is the upper layer, where optimal power flow calculations occur, and which provides the droop control with the necessary references. The second layer is lower, the droop control, which is responsible for stabilizing the DC voltage across the system.

In voltage source converter-based HVDC systems, several techniques have been proposed to solve the OPF problem. The second-order cone programming (SOCP) method was used in [50], where the active power of the converter determines its losses while the work conducted in [51] compared SOCP to SDP relaxation technique for DC systems. Furthermore, the SOCP relaxation method has solved the OPF in resistive networks in comparison with the SDP approach [52]. In [53], the sequential quadratic programming method was implemented to solve the OPF in HVDC-connected offshore wind farms. The interior point method was presented in [54] and [55] while the Newton-Raphson algorithm was studied in [56].

Using the aforementioned methods, it is difficult to obtain a global optimal solution from local optimal solutions. As a consequence, the SDP technique has been drawing considerable attention in recent years. In [57], the SDP relaxation technique was used to solve the OPF for cyclic networks, especially weakly-cyclic networks. The author in [58] presented the OPF formulation for both the bus injection model (BIM) and the branch flow model (BFM) as well as to prove that these two models are equivalent. In [59], the OPF problems was solved for AC-DC grids, including converter losses, and a modified IEEE 118-bus test system was used to approve the results. The necessary conditions for SDP in radial and meshed networks have also been investigated in an attempt to solve the OPF problem [60]. The dual problem of a reformulated OPF problem was presented in [61] as an SDP optimization where the duality gap is zero. In [62], SDP was implemented

to decompose the joint OPF and Electric-Vehicle (EV) charging problem using a nested optimization approach. Furthermore, SDP was applied across different fields, such as economic dispatch [63], the hydrothermal coordination optimization problem [64], and unit commitment [65].

3.7.1 Primary Control

DC droop voltage control is necessary in MTDC systems since the difference in the voltage ratings among the terminals affects the power flow among them. Unlike AC systems where the same voltage ratings are used across the system, terminals of MTDC systems have various voltage levels to provoke the power flow in the DC grid. DC droop control can be defined as a combination of two control modes, namely constant power and constant voltage modes, in which the DC voltage level and the power balance are maintained throughout the system. From the DC voltage droop in Figure 3.3, the steady state equations of the droop voltage control can be described by a proportional control to maintain the DC voltage level by operating as an input to a constant power control, presented, respectively, as [66, 67]:

$$\begin{aligned} P - P_{ref} &= k(V_{ref} - V) \\ V &= V_{ref}\left(\frac{P_{ref} - P}{k}\right) \end{aligned} \tag{3.8}$$

where V_{ref} and P_{ref} are the voltage and power reference values, respectively, and V and P are the measured voltage and power, respectively. k is the proportional gain which can set the ratio of the DC voltage regulation among all the droop-controlled terminals in the system, and is equal to:

$$k = \frac{P_{rated}}{V_{rated} \cdot \lambda} \tag{3.9}$$

where P_{rated} and V_{rated} represent the rated power and voltage of the droop-controlled station. λ is the slope in Figure 3.3 that donates the ratio of the DC voltage change to the

power change forming the droop gain. In the previous equations, the DC voltage references are updated using a secondary OPF control in order to fulfill a multi-objective function.

The case illustrated in Figure 3.3 is the basic operation principle of DC voltage droop control whereby the system has four terminals in which VSC1 and VSC2 are droop-controlled stations, while VSC3 and VSC4 work as constant power stations. This system works at point A with a set equilibrium where $P_1 + P_2 = P_3 + P_4$ correspond to V_1^A and V_2^A. When VSC3 and VSC4 start injecting more power, droop-controlled terminals shift the system to a new equilibrium at point B, which leads the DC voltage to increase. Therefore, VSC1 and VSC2 have to adapt to the new level of power, and change their power share contribution percentage. To the contrary, when the DC voltage drops, VSC1 and VSC2 increase the amount of injected power to the DC grid.

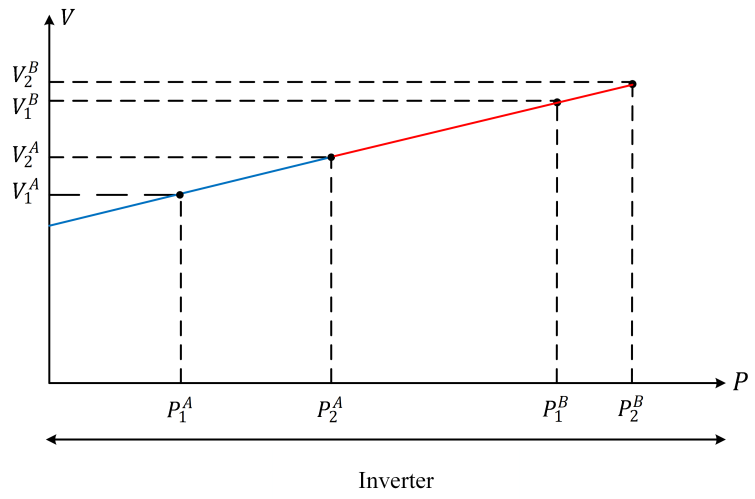

Figure 3.3: Droop control

3.7.2 Secondary Control

One of the main advantages of MTDC systems is the efficient transmission of power, especially renewable-produced power, over long distances. Efficiency is achieved by minimizing the transmission line and converter losses that are used in the process. As a result, minimizing these losses is included in the objective function of the secondary level control. A significant difference between the OPF and traditional power flow is the former's ability to control the system using both equality and inequality constraints, and the basic form of OPF is:

$$Min\, f(\underline{u}, \underline{x}) \tag{3.10}$$

subject to

$$\underline{g}(\underline{u}, \underline{x}) = \underline{0}$$
$$\underline{h}(\underline{u}, \underline{x}) \leq \underline{0}$$

where

$\underline{u}$ = vector of m control variables

$\underline{x}$ = vector of n state variables

$f : \Re^m \times \Re^n \rightarrow \Re$ is the objective functions

$\underline{g} : \Re^m \times \Re^n \rightarrow \Re^n$ is the equality constraints function

$\underline{h} : \Re^m \times \Re^n \rightarrow \Re^n$ is the inequality constraints function

The objective function of this OPF problem includes the generation cost and the total losses of the system. The generation cost function $C_i(P_i)$ can be addressed by a quadratic function.

$$G_{cost} = \sum_{i=1}^{NG} C_i(P_i) = \sum_{i=1}^{n} a_i P_i^2 + b_i P_i + c_i \tag{3.11}$$

where i is the number of the generator and NG is the total number of generators in the system, including the slack bus, whereas P_i represents the amount of active power at bus i. The number of buses is N, and a_i, b_i, and c_i express the positive coefficients of the quadratic function. In the following equations, capital letters define matrices while lower letters are variables or constants. The total losses of the system are essentially the difference between the total power injected at the generation side and the total power received at the demand side. Specifically, the total losses in this model are a summation of line losses as well as AC/DC converter losses.

$$P_{total\,loss} = \sum_{i=1}^{n} C_i(P_i) - P_{d_i} \tag{3.12}$$

$$= \sum_{x=1}^{N}\sum_{z=1}^{N} y_{xz} v_x v_z + \sum_{ac\in T} p_{ac} \tag{3.13}$$

where T is the number of AC/DC terminals ($T \subseteq N$), the DC admittance matrix is defined by Y, and the HVDC lines are addressed by $(x, z) \subseteq N \times N$. Many equations and constraints affect Equation 3.13; they are as follows:

$$p_{ac} = \sum_{a\in T} a + \beta \cdot I_c + \gamma \cdot I_c^2 \tag{3.14}$$

$$I_c = \frac{\sqrt{P_c^2 + Q_c^2}}{\sqrt{3}V_c} \tag{3.15}$$

$$v_1 = 1 \tag{3.16}$$

$$p_{in} = \sum_{x=1}^{N}\sum_{z=1}^{N} y_{xz} v_x v_z \tag{3.17}$$

$$h_{xz} = \frac{v_x^2 - (v_x - v_z)}{z_{xz}} \tag{3.18}$$

$$-h_{xz(max)} \leq h_{xz} \leq h_{xz(max)} \tag{3.19}$$

$$v_{min} \leq v \leq v_{max} \tag{3.20}$$

$$p_{in_{min}} \leq p_{in} \leq p_{in_{max}} \tag{3.21}$$

where Equation 3.14, and Equation 3.15 are the AC/DC converter losses, and the converter current, respectively, as previously mentioned in subsection 3.6.6. The slack bus voltage is addressed in Equation 3.16 ,while Equation Equation 3.17 is the power balance equation in terms of the injected power of the AC/DC converter. Equation 3.18 is the power flowing through the HVDC lines, and the constraints on the power flowing through these lines are defined by Equation 3.19. The acceptable voltage and power bounds on the AC/DC converter are represented by Equation 3.20, and Equation 3.21, respectively.

Therefore, the objective function of the model is:

$$f = G_{cost} + P_{total\,loss} \tag{3.22}$$

This multi-objective function is subject to a set of equality and inequality constraints that are listed and explained below:

$$P_i - PD_i = \sum_{j=1}^{n} |V_i||V_j||Y_{ij}|cos(\theta_{ij} + \delta_j - \delta_i), i \neq j, \forall i \in N \tag{3.23}$$

$$Q_i - QD_i = -\sum_{j=1}^{n} |V_i||V_j||Y_{ij}|sin(\theta_{ij} + \delta_j - \delta_i), i \neq j, \forall i \in N \tag{3.24}$$

where P_i and Q_i are active and reactive power generated at bus i, and PD_i and QD_i are the demand active and reactive power at bus i, respectively. The voltage magnitudes at bus i and j are represented by V_i and V_j , respectively, and Y_{ij} is the admittance between buses i and j. θ and δ are the angles of the Y parameters and bus voltage in the model, respectively. The following inequality constraints include the generator active and reactive power limits, voltage magnitude, and the bound on apparent power.

$$P_i^{Min} \leq P_i \leq P_i^{Max}, \forall i \in NG \tag{3.25}$$

$$Q_i^{Min} \leq Q_i \leq Q_i^{Max}, \forall i \in NG \tag{3.26}$$

$$V_i^{Min} \leq |V_i| \leq V_i^{Max}, \forall i = 1, ..., N \tag{3.27}$$

$$|S_{ft}| \leq S_{ft}^{Max} \tag{3.28}$$

The problem of nonlinearity and non-convexity can be seen above in both equations and constraints. Applying traditional solving techniques does not guarantee the global solution for which SDP is formulated and investigated. SDP is a technique that uses a symmetric matrix in order to optimize a linear objective function that is subject to linear constraints, the main constraint of which is that the matrix has to be positive semidefinite. This algorithm has the edge over many methods in terms of ability to handle a large number of variables and the time required to solve the problem. Furthermore, its capability to achieve a global solution is considered as the most important advantage. These combined features have resulted in increased research and employment of SDP in power systems. The basic formulation of SDP is [68]:

$$Minimize \quad Trace(C \cdot W) \tag{3.29}$$

subject to

$$A \cdot W = B \tag{3.30}$$

$$W \trianglerighteq 0 \tag{3.31}$$

where C represents the losses, or is selected based on the objective function, and W is the key variable, which is a positive and asymmetric matrix ($\trianglerighteq$), unlike linear programming where the optimization variable is a vector. The constraints are represented by A and B.

Two cases in this section are modelled and investigated, the first of which is the SDP formulation of OPF, regardless of the AC/DC converter losses. The matrix W needs to be

defined:

$$W = X \cdot X^T \tag{3.32}$$

where W is a rank one positive and a symmetric matrix, and X is a column vector.

The objective function in SDP terms is:

$$P_{total\,loss} = Tr(Y \cdot W) \tag{3.33}$$

subject to

$$(v_{min})^2 \cdot \widehat{O} \leq W \leq (v_{max})^2 \cdot \widehat{O} \tag{3.34}$$

$$P_{in} = Diag(Y \cdot W) + (D \cdot M_{inc}) \tag{3.35}$$

$$H = A(D) \cdot vec(W) \tag{3.36}$$

$$P_{in_{min}} \leq P_{in} \leq P_{in_{max}} \tag{3.37}$$

$$-H_{max} \leq H \leq H_{max} \tag{3.38}$$

$$rank(W) = 1 \tag{3.39}$$

$$W \succeq 0 \tag{3.40}$$

where p_{in}, and h_{xz}, as previously mentioned, act as entries for column vectors P_{in} and H. $\widehat{O}$ is an all-one matrix, $Diag$ represents the main diagonal, and M_{inc} is a reduced incidence matrix, whereas $A(D)$ is a matrix that complies with Equation 3.18.

The second case that is investigated is that the AC/DC converter losses are added to the objective function.

$$p_{total\,loss} = Tr(Y \cdot W) + P_{ac} \tag{3.41}$$

subject to

$$(v_{min})^2 \cdot \widehat{O} \leq W \leq (v_{max})^2 \cdot \widehat{O} \tag{3.42}$$

$$H = A(D) \cdot vec(W) \tag{3.43}$$

$$p_{ac} \geq \alpha + \beta \cdot I_c + \gamma \cdot I_c^2 \tag{3.44}$$

$$P_{in} = Diag(Y \cdot W) + (D \cdot M_{inc}) + P_{ac} \tag{3.45}$$

$$P_{in_{min}} \leq P_{in} \leq P_{in_{max}} \tag{3.46}$$

$$-H_{max} \leq H \leq H_{max} \tag{3.47}$$

$$rank(W) = 1 \tag{3.48}$$

$$W \trianglerighteq 0 \tag{3.49}$$

Chapter 4

Simulation Results

In this chapter, an optimal power-sharing control is presented and tested. The control strategy implements a voltage droop control and an OPF as a lower and upper control, respectively, in which the OPF algorithm optimizes the droop values to reach an optimal power sharing, and to meet the multi-objective function. These objectives include minimizing the losses of transmission lines and converters using the SDP algorithm in order to obtain a global solution, unlike other techniques that achieve local solutions. This chapter will cover the dynamics of the system, including the DC voltage, active power, and the accuracy of power sharing during steady state and transient situations. The simulation results were simultaneously modelled and tested in PSCAD/EMTDC and Matlab environments in which the primary control and HVDC components were modelled in PSCAD, while the secondary control was executed in Matlab as shown in Figure 4.1.

A modified CIGRE B4 DC grid test system was used to test the proposed control method [2]. This system consists of five VSC terminals and long transmission DC lines forming a MTDC grid, as shown in Figure 4.2. Three VSC stations, designated as VSC1,

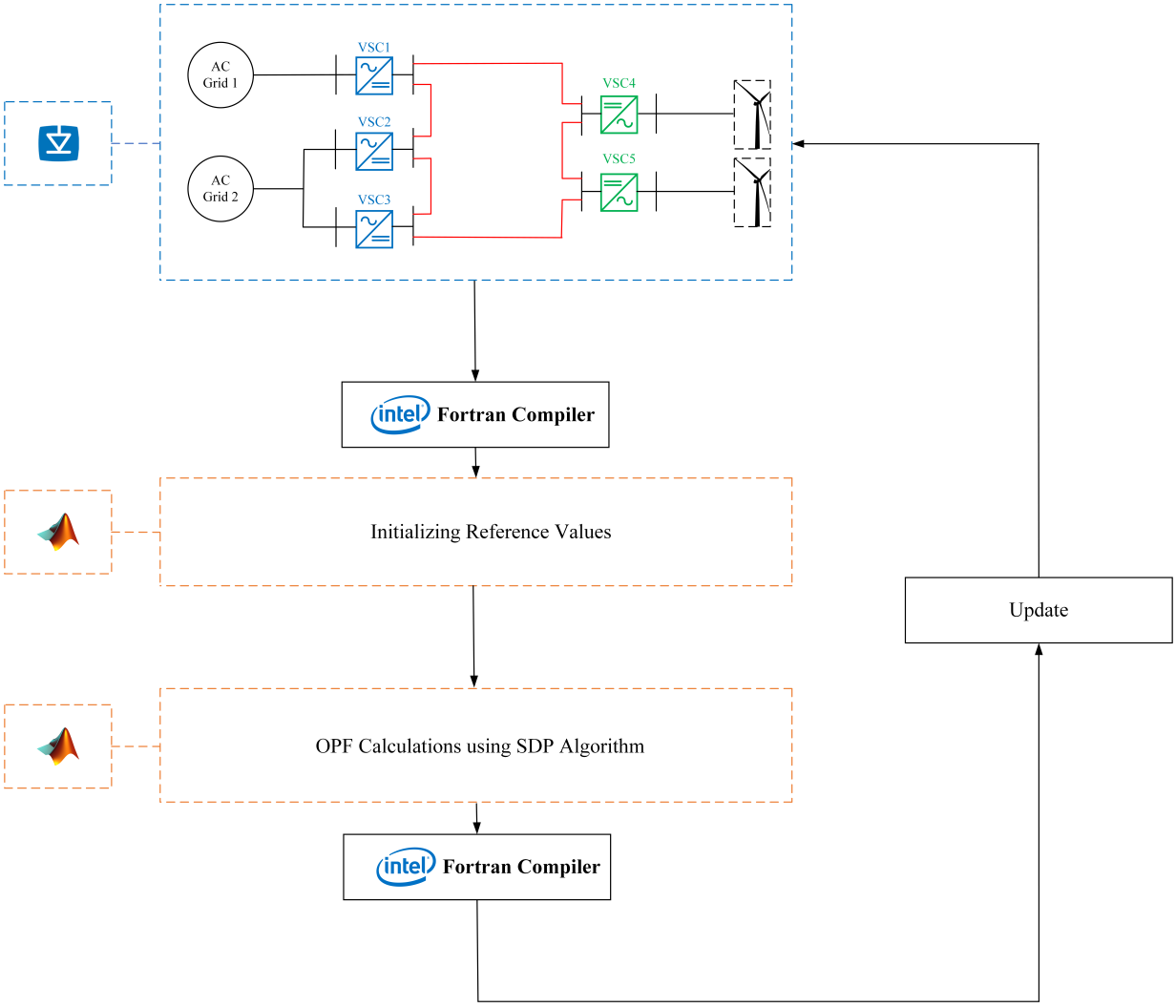

Figure 4.1: Matlab and PSCAD/EMTDC co-simulation setup

VSC2, and VSC3, are set to operate as constant DC voltage regulators under the droop control method and in an inversion mode. These three converters link the main onshore AC grid with the DC grid, and have to balance the difference between the generators and the loads of the system. However, the other two terminals, designated as VSC4 and VSC5, which are wind farms that are connected to offshore AC buses, operate as constant active

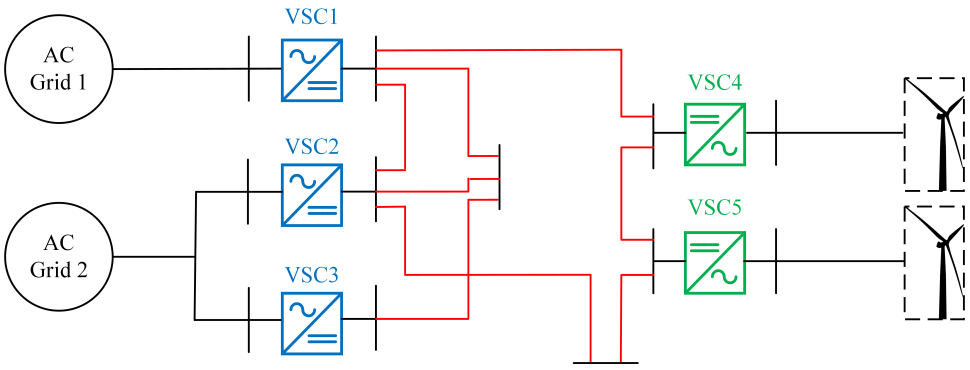

Figure 4.2: A modified CIGRE B4 DC grid test system [2]

power control stations and in a rectification mode. The droop-controlled terminals in the system are connected to stiff AC systems where the AC voltage level at the PCC is constant regardless of the magnitude and direction of active and reactive power. These systems are modelled by an ideal three-phase AC source. The other terminals are connected to offshore AC buses in order to integrate offshore wind farms that work as constant-power sources. The proposed control scheme is verified and compared in this chapter based on three cases: operating under voltage droop control only; applying both primary and secondary control; and performing under an outage in one of the droop-controlled terminals. In all cases, three factors are the main focus of this thesis, namely DC voltage level, active power flow, and the losses of transmission lines and converters. Specifically, the DC voltage level is the most important since it is the validation of stability in MTDC systems. Table 4 shows the parameters of the MTDC system, including voltage and power ratings as well as lines.

The tuning process of the system controllers, as mentioned in Chapter 2, is explained as follows:

The inner current controller uses the modulus optimum method to tune the PI controllers in order to achieve a fast response in terms of input reference values. The integral

Table 4.1: Parameters of the MTDC System

Parameter	Value
Converter Rated Power	100 MVA
Line-Line Voltage	24.5 KV_{rms}
DC Voltage	50 KV
AC Side Resistance	0.06 Ω
AC Side Inductance	0.0048 H
DC Side Capacitance	400 μF
Switching Frequency	5 KHz

time constant T_c is calculated based on Equation 2.64:

$$T_c = 0.0133s \tag{4.1}$$

The proportional gain of the controller is determined by Equation 2.63:

$$K_{pi} \approx 4 \tag{4.2}$$

The controllers of active and reactive power are tuned by the symmetrical optimum method where the the integral time constant T_v and the proportional gain K_{pi} are based on Equation 2.89, and Equation 2.91, respectively:

$$T_v \approx 0.0266s \tag{4.3}$$

$$K_{pi} = 0.43 \tag{4.4}$$

In the following cases, the system has a good transient response performance due to the accurate tuning of PI controllers which cancels the need for a start up transient control. In

this analysis, two main study cases are discussed: the first case demonstrates the behaviour of the system under the primary control only, whereas both the primary and secondary control are employed in the second case. These cases are examined according to power increase by the wind farms in steps of 50%, 80%, and 100% of the total injected power, which is 140 MW to validate the proposed control approach.

4.1 Case I: Using Primary Control Only Under Normal Operations

This case solely operates under primary control which implies that the power sharing between all the terminals is governed by the droop gains. All the bus system work at their nominal voltage initially, which leads to no power flow in the system from 0 s until 0.5 s. The active power delivered to the DC grid by the input power converters VSC4 and VSC5 is shared among the voltage droop-controlled terminals according to the following percentages: 40%, 40%, and 20% for VSC1,VSC3, and VSC2, respectively.

At 0.5 s, VSC4 and VSC5 inject a total power of 70 MW, which causes a power imbalance that results in a voltage deviation in the system. In this case, this deviation triggers only the voltage droop control at the lower level of the control scheme. The power shared between VSC1,VSC2, and VSC5 is determined by the droop gain of each terminal, which is not equal in this case.

At 3.5 s, VSC4 and VSC5 starts to increase their total power to 30% in addition to the existing 50%. This increase affects the contribution of the droop-controlled terminals in terms of the power sharing level and system stability by reaching a new equilibrium point.

At 6.5 s, VSC4, and VSC5 reach the maximum injected power, which is 140 MW.

VSC1, VSC2 and VSC3 keep the system stable regarding the DC voltage and power flow among the terminals, despite the changes in loads. The droop-controlled stations work constantly in order to adapt to the new level of power sharing with the dual aim of equal power sharing and keeping a constant DC voltage at 50 kV until the end of the simulation time 10 s.

The voltage is constant and stable throughout the MTDC system during the scenario, as can be seen in Figure 4.3. This is a reflection of the system stability, dynamics, and the ability to adapt by reaching a new equilibrium point at each case. The changes of power, and voltage in VSC1, and VSC3, and the power sharing among the droop-controlled terminals, are shown in Figure 4.3, Figure 4.4, Figure 4.5, and Figure 4.6. Table shows all the scenarios, including the voltage and power values across the system.

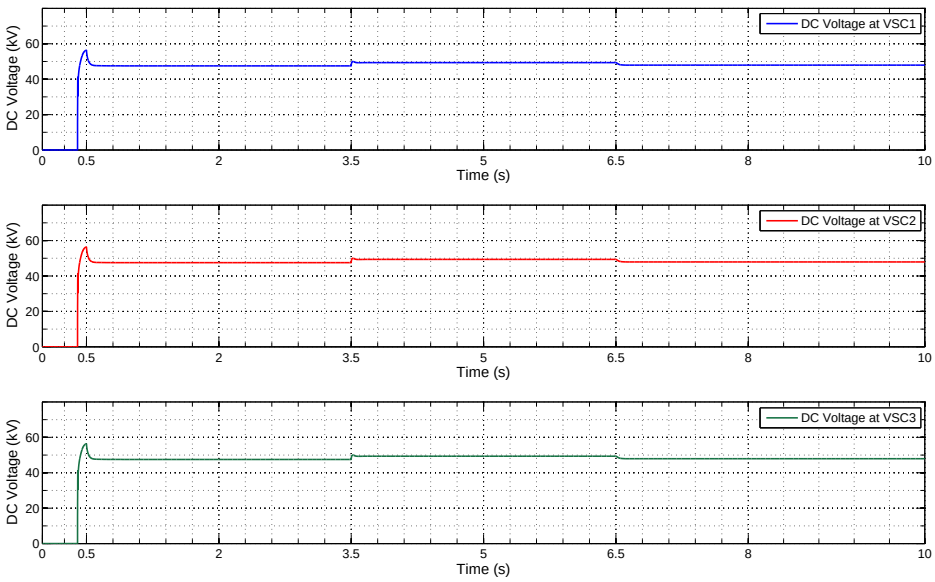

Figure 4.3: Voltage level at VSC1, VSC2, and VSC3 in Case 1

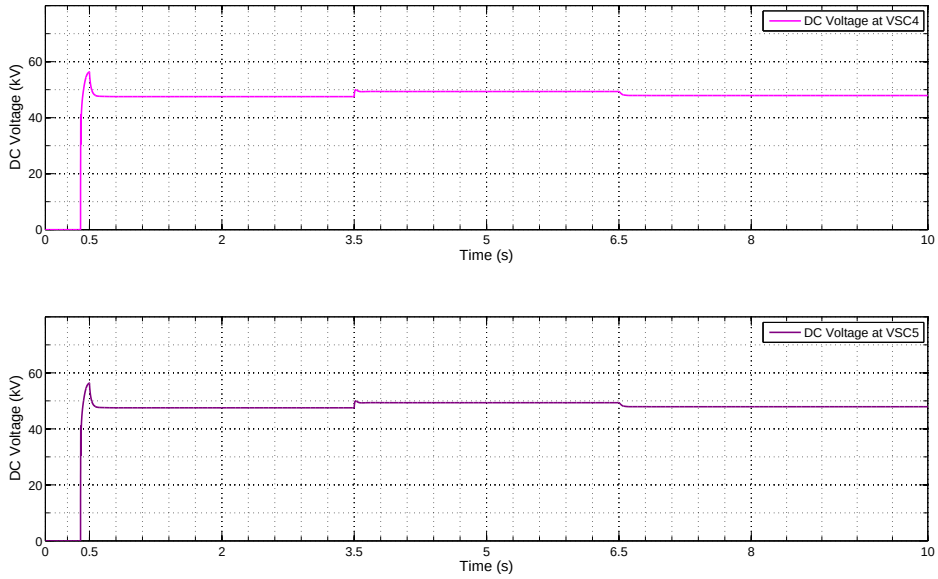

Figure 4.4: Voltage level at VSC4, and VSC5 in Case 1

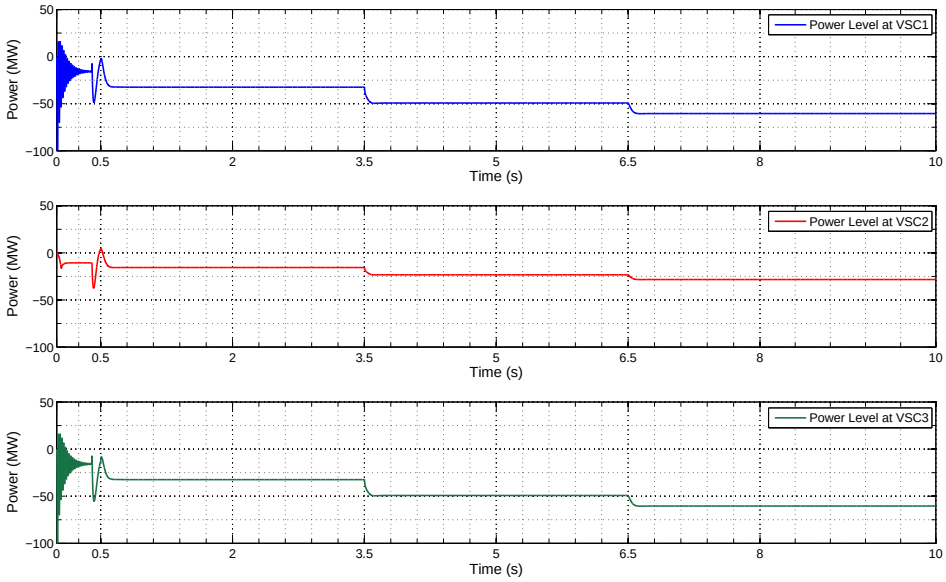

Figure 4.5: Power performance at VSC1, VSC2, and VSC3 in Case 1

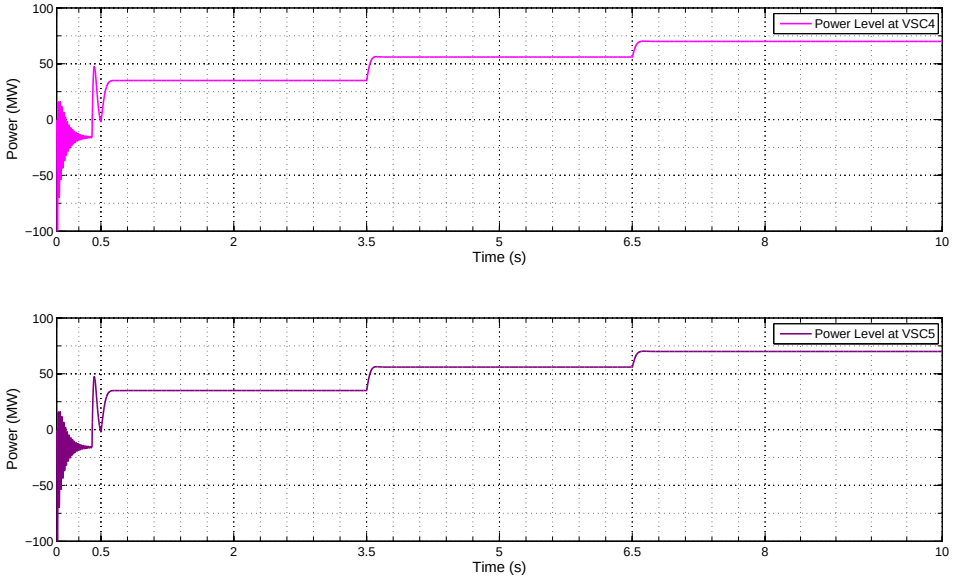

Figure 4.6: Power performance at VSC4, and VSC5

4.2 Case II: Using the Proposed Control Technique Under Normal Operations

This case illustrates the combination of the primary and secondary control in terms of operating in coordination with each other, and at the same time. The same sequence of events is implemented as the previous cases in order to show the differences when the secondary control is used. The proposed OPF in the secondary control is enabled to illustrate the arrangement between the primary and secondary control with the same sequence of actions as Case I. Moreover, the accuracy of power sharing among the terminals is investigated to examine the effect of the system losses, including the transmission lines and converters losses. The produced active power by the offshore wind farms, VSC4 and VSC5, is increased in steps until their rated power is reached. The output power terminals, VSC1, VSC2, and VSC3, share the imported power based on predefined shared values. An optimal power-sharing control requires the droop gains, and voltage reference settings to be determined according to the secondary control. This secondary control optimizes the process of power sharing by eliminating the influence of DC grid lines, and converters losses in addition to meeting a specific multi-objective function.

At $t = 0.5\ s$, terminals 4, and 5 supply power at the 50% level of the total generated power. The grid-connected terminals follow the same desired shares of power of 40%, 40%, and 20% for VSC1, VSC3, and VSC2, respectively. The controllers of these terminals receive voltage droop-reference settings according to power shares, power delivered, and the droop gains.

At $t = 3.5\ s$, 80% of the total power generated by wind farms is delivered by VSC4, and VSC5. The secondary control level updates the values of voltage references in the droop-controlled converters based on the available power in order to obtain a new equilibrium

point. The percentage of power sharing among VSC1, VSC2, and VSC3 stays the same as the agreement, despite the change in input power. Furthermore, the DC voltage level across all the terminals is kept constant, and within the acceptable limits.

At $t = 6.5\ s$, VSC4, and VSC5 now operate according to their rated power; in other words, all the generated power from the wind farms is delivered to the DC grid. The output power terminals are governed by the secondary control to achieve an accurate power-sharing percentage regardless of the sudden increase of power in the DC grid. Figure 4.7, Figure 4.8, Figure 4.9, and Figure 4.10 summarize the results of the case across the system parameters.

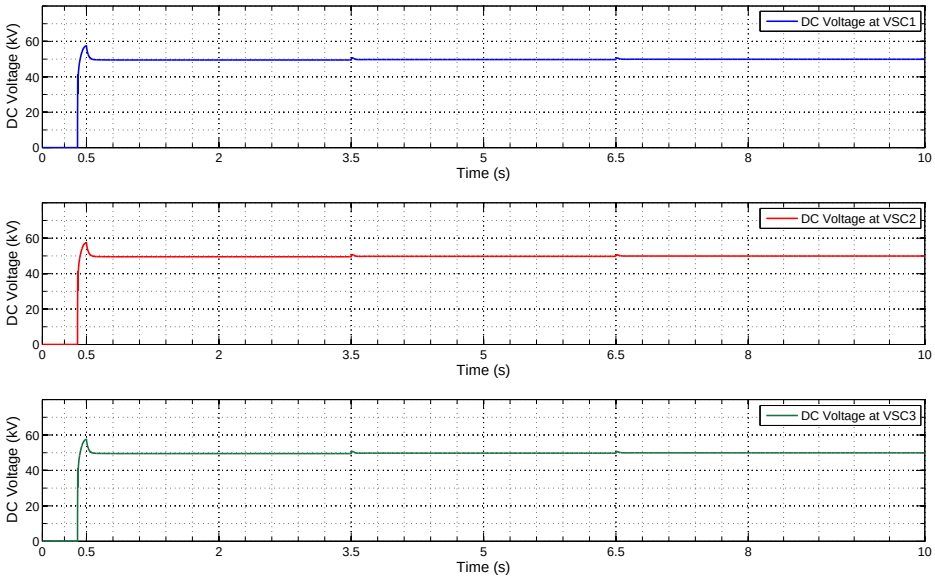

Figure 4.7: Voltage level at VSC1, VSC2, and VSC3

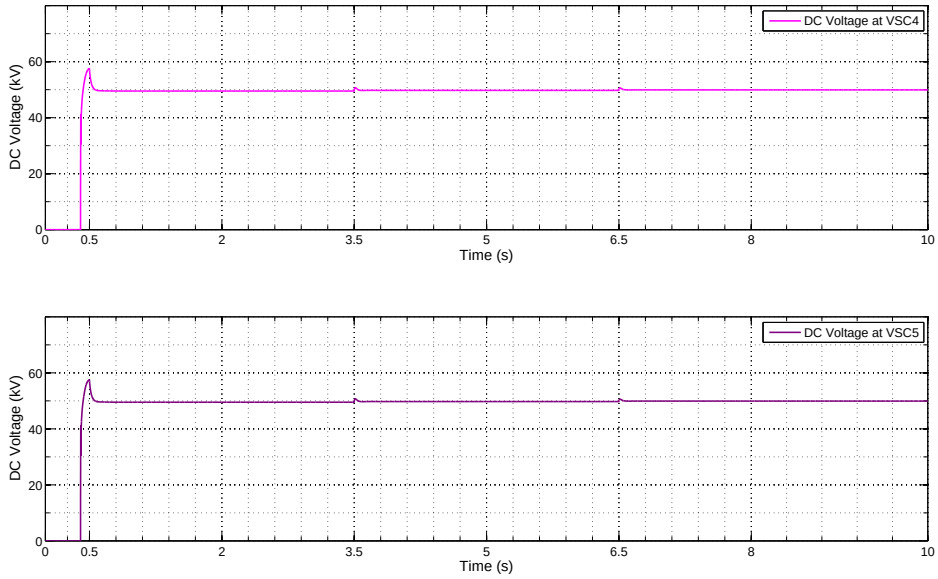

Figure 4.8: Voltage level at VSC4, and VSC5

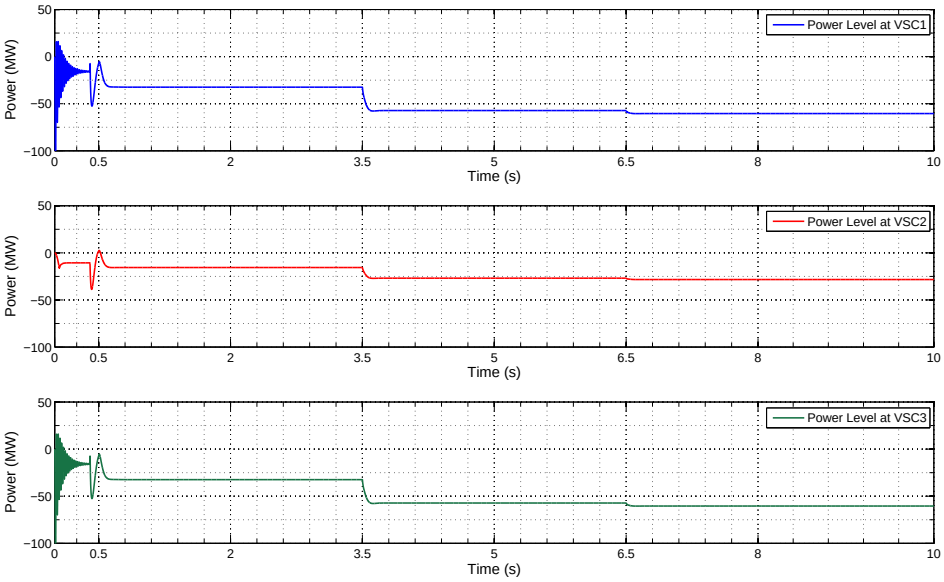

Figure 4.9: Power performance at VSC1, VSC2, and VSC3

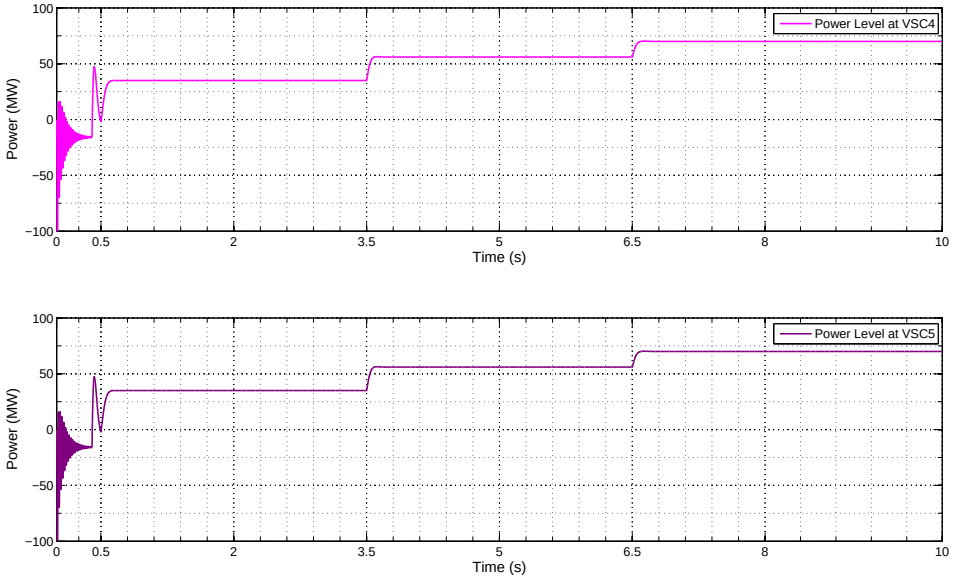

Figure 4.10: Power performance at VSC4, and VSC5

4.2.1 Using the Proposed Control for Equal Power Sharing

In this case, equal power sharing is implemented between the droop-controlled terminals where the same sequence of events as the previous case is used to test the system. It starts with all the terminals working under theoretical voltage ratings but, after 0.5 s, 50% of the injected power from the wind farms is switched on at VSC4 and VSC5. These terminals then produce an extra 30% at 3.5 s in which the droop gains of VSC1, VSC2 and VSC3 are set to share the power equally and maintain a good performance through the variations of power from the wind farms terminals. The performance of the voltage and power in the grid is summarized in table and in Figure 4.11, Figure 4.12, Figure 4.13, and Figure 4.14. The effect of changing the load in steps can also be seen. The values of power sharing among VSC1, VSC2, and VSC3 agree with the theoretical estimation.

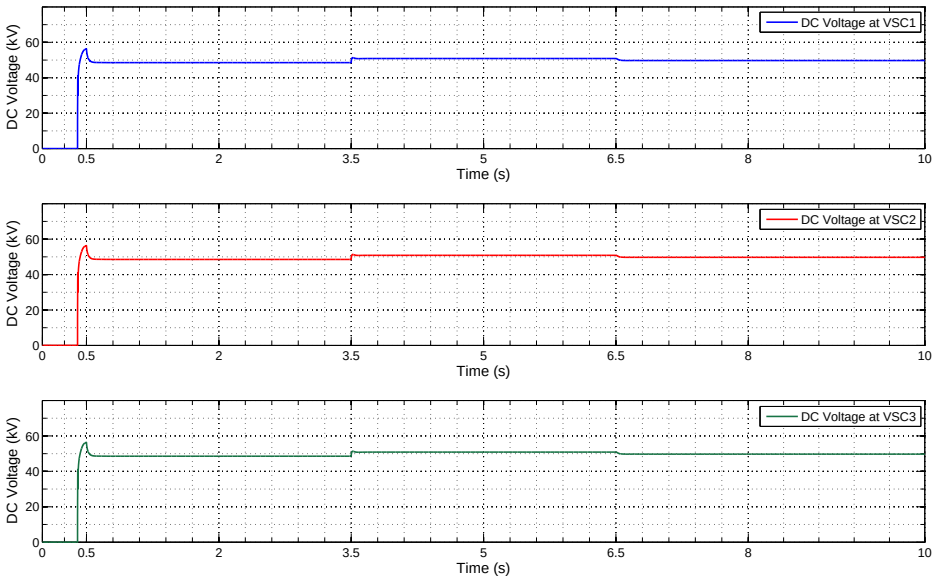

Figure 4.11: Voltage level at VSC1, VSC2, and VSC3

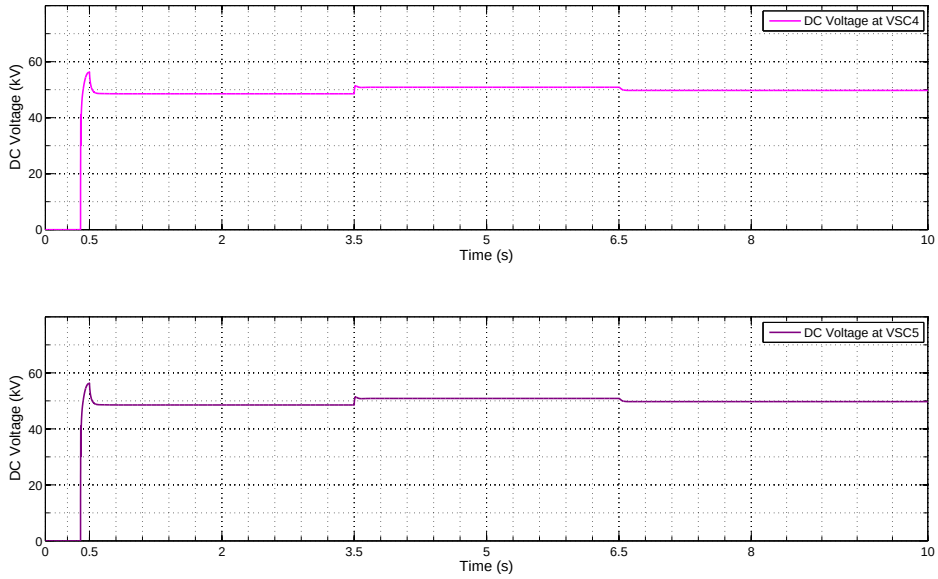

Figure 4.12: Voltage level at VSC4, and VSC5

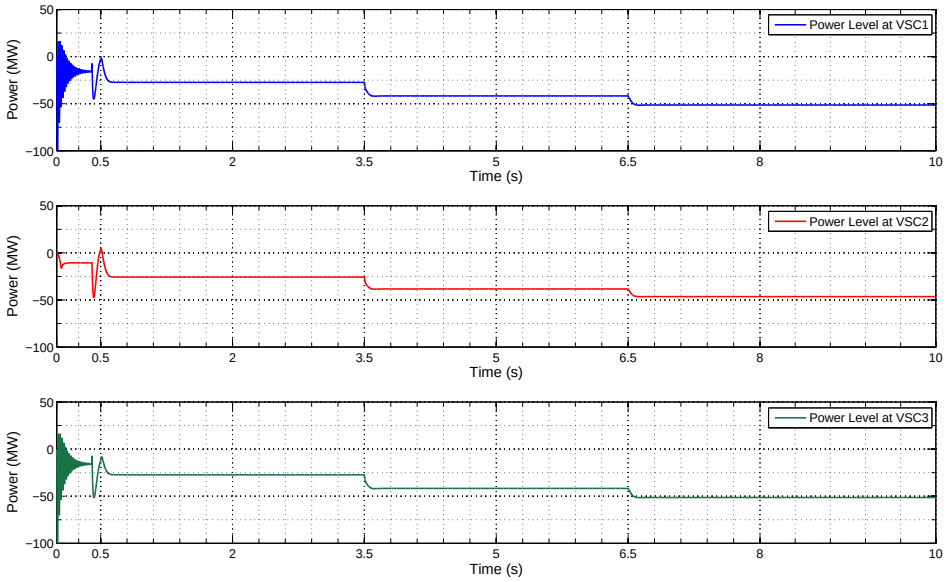

Figure 4.13: Power performance at VSC1, VSC2, and VSC3

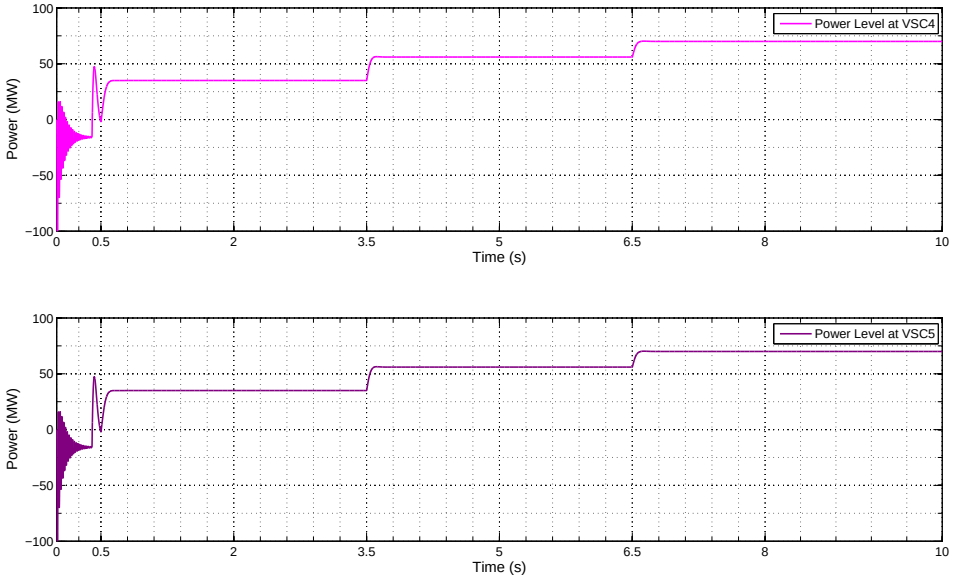

Figure 4.14: Power performance at VSC4, and VSC5

4.2.2 Using the Proposed Control During a Terminal Outage

This case study is a demonstration of the system behaviour during an unexpected terminal outage where the DC voltage level, power sharing among droop-controlled terminals, and the overall stability of the system are investigated. The case follows the same sequence of actions as the first case except at 3.5 s when VSC3 is disconnected from the system. A terminal outage in MTDC systems is defined as one where the terminal stops consuming power, which leads the other terminals to consume power and operate at their maximum ratings. This case shows the stability of the system in terms of keeping a constant DC voltage and sharing power based on the predefined droop gains, as shown in Figure 4.15, Figure 4.16, Figure 4.17, and Figure 4.18. The system is still in a continuous state from Case I and it can be seen that VSC1 and VSC2 are in control of the power sharing percentage of VSC3 at the moment when it is out of the system. Although the voltage level across the grid is distributed, it is sustained within the acceptable limits. At 6.5 s, VSC3 is back online, and the system now operates based on the droop gain in terms of power sharing. The voltage ratings remain stable.

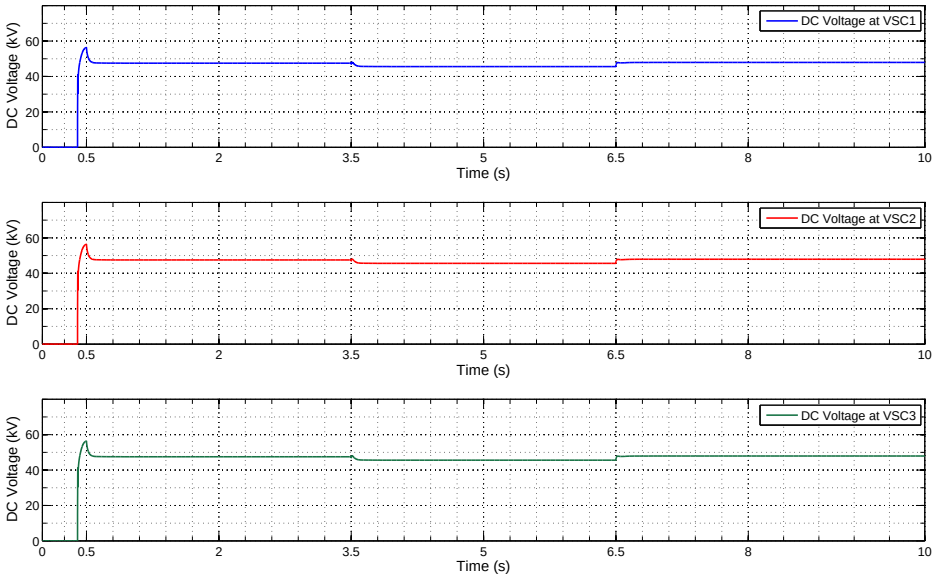

Figure 4.15: Voltage level at VSC1, VSC2, and VSC3

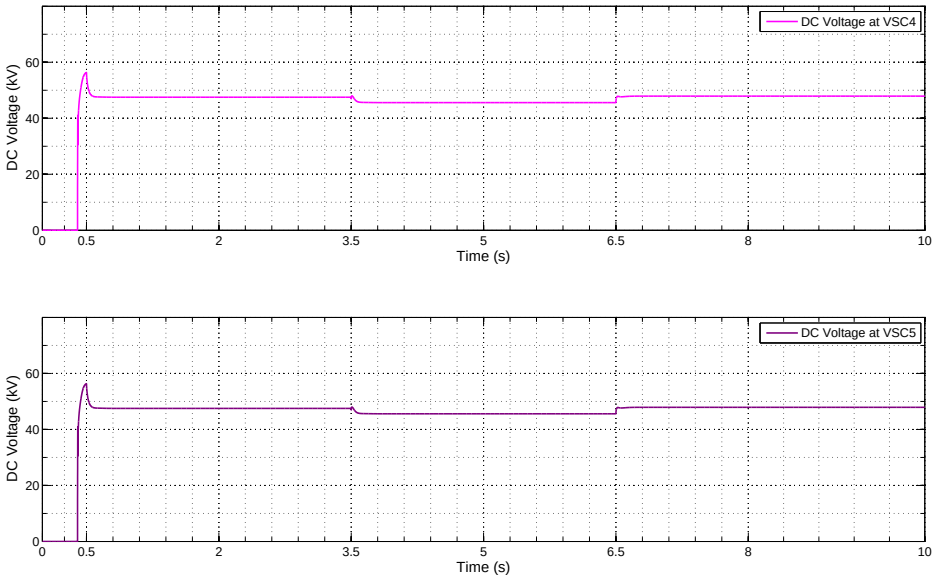

Figure 4.16: Voltage level at VSC4, and VSC5

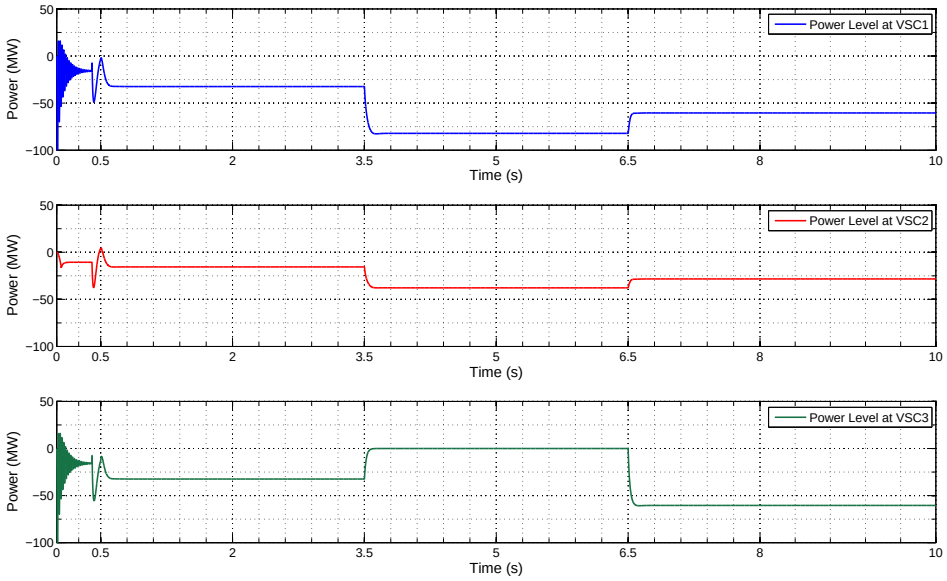

Figure 4.17: Power performance at VSC1, VSC2, and VSC3

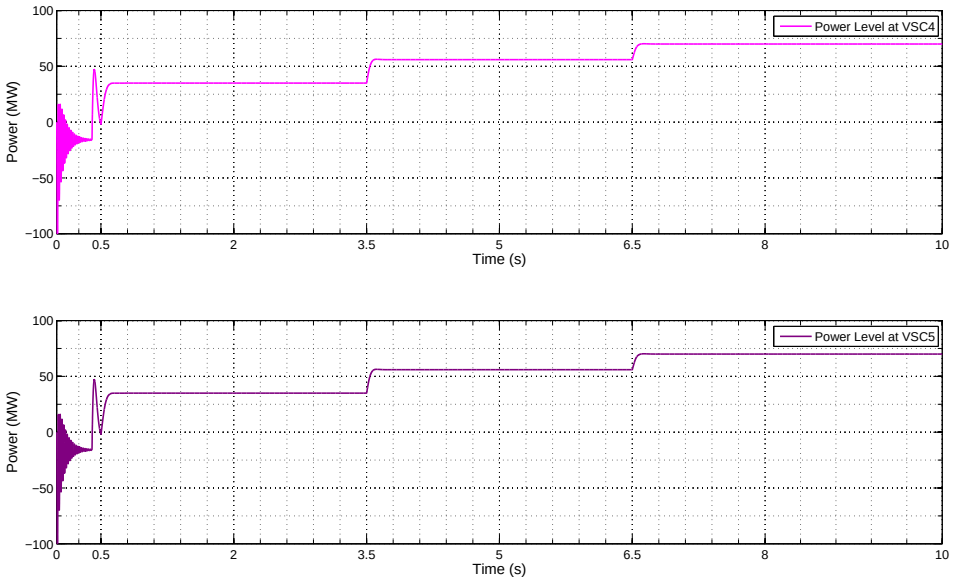

Figure 4.18: Power performance at VSC4, and VSC5

Chapter 5

Conclusion and Future Work

5.1 Conclusion

This thesis proposes an optimal power sharing control of MT-HVDC VSC-based systems using a hierarchical control structure in which DC voltage droop control is implemented at the primary level, and SDP is used at the secondary level of the control. The proposed control technique aims at reaching an accurate power sharing among MTDC terminals while considering the losses of converters, and transmission lines. From the device level, the VSC is addressed in terms of the operational process and the main components. In addition, the VSC station is described thoroughly in a mathematical model to obtain a better understanding of the power flow between the main AC grid and the DC grid through the VSC terminal. The control aspect of HVDC VSC-based systems has also been proven in order to achieve an independent control of the active and reactive power that is considered to be one of the most important advantages of the VSC. This occurs using a cascade control scheme that consists of an inner current controller, PI, and outer controllers. One of the

main targets of this thesis, namely the losses of the converters, are studied based on each component of the VSC as well as a generalized loss model. From the system level, power sharing techniques among MTDC terminals are discussed and compared resulting in the adoption of a DC voltage droop control as the primary control in the system. A secondary control is based on the SDP optimization method whose model has been modified to add the transmission lines, and converters losses into the formulation. Simulation results show the verification of the proposed control scheme for MTDC systems with the integration of offshore wind farms. This control scheme is tested in terms of efficiency and robustness by applying a power increase in steps, and a terminal failure. These conditions demonstrate the stability of the system alongside the accuracy of power sharing, and the constant level of DC voltage. This thesis uses a modified CIGRE B4 DC grid test system that consists of two offshore wind farms and three droop-controlled terminals connected to onshore AC grids. The proposed control has been simultaneously simulated in the PSCAD/EMTDC and Matlab environments.

5.2 Future Work

- Applying the proposed control technique to a larger scale test system as well as different configurations of HVDC systems.
- Studying the effect of using unbalanced AC sources since the AC side in this thesis is considered to be a balance AC source.

References

[1] WindEurope. Wind energy in Europe in 2018, Trends and statistics. Technical report, WindEurope, 2018.

[2] CIGRE B4 Working Group. The CIGRE B4 DC Grid Test System. (270):10–19, 2013.

[3] Xiaodong Liang. Emerging Power Quality Challenges Due to Integration of Renewable Energy Sources. *IEEE Transactions on Industry Applications*, 53(2):855–866, 2017.

[4] Eurostats. Renewable energy statistics Highlights. Technical Report January 2019, 2019.

[5] Sílvio Rodrigues, Rodrigo Teixeira Pinto, Pavol Bauer, and Jan Pierik. Optimal power flow control of VSC-based multiterminal DC network for offshore wind integration in the North Sea. *IEEE Journal of Emerging and Selected Topics in Power Electronics*, 1(4):260–268, 2013.

[6] Nilanjan Ray Chaudhuri, Balarko Chaudhuri, Rajat Majumder, and Amirnaser Yazdani. *Multi-Terminal Direct-Current Grids*. John Wiley & Sons, Inc, Hoboken, NJ, USA, sep 2014.

[7] Wang Feng, Anh Le Tuan, Lina Bertling Tjernberg, Anders Mannikoff, and Anders Bergman. A new approach for benefit evaluation of multiterminal VSC-HVDC using a proposed mixed AC/DC optimal power flow. *IEEE Transactions on Power Delivery*, 29(1):432–443, 2014.

[8] Paola Bresesti, Wil L. Kling, Ralph L. Hendriks, and Riccardo Vailati. HVDC Connection of Offshore Wind Farms to the Transmission System. *IEEE Transactions on Energy Conversion*, 22(1):37–43, mar 2007.

[9] Shu Wang, Jinxiang Zhu, Lan Trinh, and Jiuping Pan. Economic assessment of HVDC project in deregulated energy markets. In *2008 Third International Conference on Electric Utility Deregulation and Restructuring and Power Technologies*, pages 18–23. IEEE, apr 2008.

[10] Olof Heyman. HVDC Light ® It's time to connect. Technical report, ABB, 2012.

[11] Aishling Reidy and Rick Watson. Comparison of VSC based HVDC and HVAC interconnections to a large offshore wind farm. *2005 IEEE Power Engineering Society General Meeting*, 1(1):1–8, 2005.

[12] Hongzhi Liu and Zhe Chen. Contribution of VSC-HVDC to Frequency Regulation of Power Systems with Offshore Wind Generation. *IEEE Transactions on Energy Conversion*, 30(3):918–926, 2015.

[13] Catalin Gavriluta, Ignacio Candela, Costantino Citro, Alvaro Luna, and Pedro Rodriguez. Design considerations for primary control in multi-terminal VSC-HVDC grids, 2015.

[14] Nikolas Flourentzou, Vassilios G. Agelidis, and Georgios D. Demetriades. An overview VSC-Based HVDC Power Transmission Systems :. 24(APRIL 2009):592–602, 2015.

[15] Nilanjan Ray Chaudhuri, Balarko Chaudhuri, Rajat Majumder, and Amirnaser Yazdani. *Multi-Terminal Direct-Current Grids: Modeling, Analysis, and Control*. John Wiley & Sons, Inc, Hoboken, NJ, USA, sep 2014.

[16] Mohamadreza Baradar and Mehrdad Ghandhari. A multi-option unified power flow approach for hybrid AC/DC grids incorporating multi-terminal VSC-HVDC. *IEEE Transactions on Power Systems*, 28(3):2376–2383, 2013.

[17] H. A. Alsiraji, R. ElShatshat, and A. A. Radwan. A novel control strategy for the interlinking converter in hybrid microgrid. In *2017 IEEE Power Energy Society General Meeting*, pages 1–5, July 2017.

[18] V. Akhmatov, M. Callavik, C. M. Franck, S. E. Rye, T. Ahndorf, M. K. Bucher, H. Muller, F. Schettler, and R. Wiget. Technical guidelines and prestandardization work for first HVDC Grids. *IEEE Transactions on Power Delivery*, 29(1):327–335, 2014.

[19] Rakibuzzaman Shah, Jesus C. Sánchez, Robin Preece, and Mike Barnes. Stability and control of mixed AC-DC systems with VSC-HVDC: A review. *IET Generation, Transmission and Distribution*, 12(10):2207–2219, 2018.

[20] Ned Mohan, Tore Undeland, and William Robbins. *Power electronics : converters, applications, and design*. John Wiley & Sons, Inc, Hoboken, NJ, USA, 3rd edition, 2003.

[21] Amirnaser Yazdani and Reza Iravani. *Voltage-Sourced Converters in Power Systems*. John Wiley & Sons, Inc., Hoboken, NJ, USA, jan 2010.

[22] Michael Bahrman and Brian Johnson. The ABCs of HVDC transmission technologies. *IEEE Power and Energy Magazine*, 5(2):32–44, mar 2007.

[23] Jiebei Zhu, Campbell D. Booth, Grain P. Adam, Andrew J. Roscoe, and Chris G. Bright. Inertia emulation control strategy for VSC-HVDC transmission systems. *IEEE Transactions on Power Systems*, 28(2):1277–1287, 2013.

[24] Jef Beerten, Stijn Cole, and Ronnie Belmans. Generalized steady-state VSC MTDC model for sequential AC/DC power flow algorithms. *IEEE Transactions on Power Systems*, 27(2):821–829, 2012.

[25] Zhanfeng Song, Yanjun Tian, Zhuo Yan, and Zhe Chen. Direct Power Control for Three-Phase Two-Level Voltage-Source Rectifiers Based on Extended-State Observation. *IEEE Transactions on Industrial Electronics*, 63(7):4593–4603, 2016.

[26] C. Bajracharya, M. Marta, S. Are, and T. Undeland. Understanding of tuning techniques of converter controllers for VSC-HVDC. *Proceedings of the Nordic Workshop on Power and Industrial Electronics (NORPIE/2008)*, page 8, 2008.

[27] Chandra Bajracharya. Control of VSC-HVDC for wind power. Master's thesis, 2008.

[28] Hasan K. Alrajhi Alsiraji and Ehab F. El Saadany. Cooperative autonomous control for active power sharing in multi-terminal VSC-HVDC. *International Journal of Process Systems Engineering*, 2(4):303, 2014.

[29] Alsiraji, Hasan. Cooperative Power Sharing control in Multi-terminal VSC-HVDC. Master's thesis, 2014.

[30] Ang Ge, Jianru Wan, Zhiwei Niu, and Bin Li. Research on current feed forward decoupling control for energy feedback and grid-connected device. *2011 4th International Conference on Power Electronics Systems and Applications, PESA 2011*, 2011.

[31] J. B. Ekanayake. Multi-terminal DC converters for connecting induction generator based distribution generation. *ICIIS 2009 - 4th International Conference on Industrial and Information Systems 2009, Conference Proceedings*, (December):466–471, 2009.

[32] Wenjuan Du, Qiang Fu, and Haifeng Wang. Comparing AC Dynamic Transients Propagated Through VSC HVDC Connection With Master-Slave Control Versus DC Voltage Droop Control. *IEEE Transactions on Sustainable Energy*, 9(3):1285–1297, 2018.

[33] Lirong Zhang, Yi Wang, and Heming Li. Coordinated control of MTDC-based microgrid with wind turbines. *Conference Proceedings - 2012 IEEE 7th International Power Electronics and Motion Control Conference - ECCE Asia, IPEMC 2012*, 3:2076–2080, 2012.

[34] Xun Wan, Yunfeng Li, and Minfang Peng. Modelling, analysis and virtual parallel resistor damping control of VSC-based DC grid using master-slave control mode. *IET Generation, Transmission and Distribution*, 12(9):2046–2054, 2018.

[35] Jef Beerten, Stijn Cole, and Ronnie Belmans. Modeling of multi-terminal vsc hvdc systems with distributed dc voltage control. *IEEE Transactions on Power Systems*, 29(1):34–42, 2014.

[36] Rodrigo Teixeira Pinto, Pavol Bauer, Sílvio F. Rodrigues, Edwin Jan Wiggelinkhuizen, Jan Pierik, and Braham Ferreira. A novel distributed direct-voltage control strategy for grid integration of offshore wind energy systems through MTDC network. *IEEE Transactions on Industrial Electronics*, 60(6):2429–2441, 2013.

[37] Eduardo Prieto-Araujo, Fernando D. Bianchi, Adrià Junyent-Ferré, and Oriol Gomis-Bellmunt. Methodology for droop control dynamic analysis of multiterminal VSC-

HVDC grids for offshore wind farms. *IEEE Transactions on Power Delivery*, 26(4):2476–2485, 2011.

[38] Lie Xu, Liangzhong Yao, and Masoud Bazargan. DC grid management of a multi-terminal HVDC transmission system for large offshore wind farms. *1st International Conference on Sustainable Power Generation and Supply, SUPERGEN '09*, pages 1–7, 2009.

[39] R. Teixeira Pinto, S. F. Rodrigues, P. Bauer, and J. Pierik. Comparison of direct voltage control methods of multi-terminal DC (MTDC) networks through modular dynamic models. *Proceedings of the 2011 14th European Conference on Power Electronics and Applications, EPE 2011*, pages 1–10, 2011.

[40] Jun Liang, Tianjun Jing, Oriol Gomis-Bellmunt, Janaka Ekanayake, and Nicholas Jenkins. Operation and control of multiterminal HVDC transmission for offshore wind farms. *IEEE Transactions on Power Delivery*, 26(4):2596–2604, 2011.

[41] Daelemans Gilles. *VSC-HVDC in meshed networks*. Master's thesis, Katholieke Universiteit Leuven, 2008.

[42] Michael Grant and Stephen Boyd. CVX: Matlab software for disciplined convex programming, version 2.1. http://cvxr.com/cvx, March 2014.

[43] Michael Grant and Stephen Boyd. Graph implementations for nonsmooth convex programs. In V. Blondel, S. Boyd, and H. Kimura, editors, *Recent Advances in Learning and Control*, Lecture Notes in Control and Information Sciences, pages 95–110. Springer-Verlag Limited, 2008. http://stanford.edu/~boyd/graph_dcp.html.

[44] Kumars Rouzbehi, Arash Miranian, Jose Ignacio Candela, Alvaro Luna, and Pedro Rodriguez. A generalized voltage droop strategy for control of multiterminal DC grids. *IEEE Transactions on Industry Applications*, 51(1):607–618, 2015.

[45] Haifeng Li, Chongru Liu, Gengyin Li, and Reza Iravani. An Enhanced DC Voltage Droop-Control for the VSC - HVDC Grid. *IEEE Transactions on Power Systems*, 32(2):1520–1527, 2017.

[46] Agustí Egea-Alvarez, Fernando Bianchi, Adrià Junyent-Ferre, Gabriel Gross, and Oriol Gomis-Bellmunt. Voltage control of multiterminal VSC-HVDC transmission systems for offshore wind power plants: Design and implementation in a scaled platform. *IEEE Transactions on Industrial Electronics*, 60(6):2381–2391, 2013.

[47] Catalin Gavriluta, Ignacio Candela, Alvaro Luna, Antonio Gomez-Exposito, and Pedro Rodriguez. Hierarchical Control of HV-MTDC Systems With Droop-Based Primary and OPF-Based Secondary. *IEEE Transactions on Smart Grid*, 6(3):1502–1510, 2015.

[48] Catalin Gavriluta, Raphael Caire, Antonio Gomez-Exposito, and Nouredine Hadjsaid. A Distributed Approach for OPF-Based Secondary Control of MTDC Systems. *IEEE Transactions on Smart Grid*, 9(4):2843–2851, 2018.

[49] Minxiao Han, Dong Xu, and Lei Wan. Hierarchical optimal power flow control for loss minimization in hybrid multi-terminal HVDC transmission system. *CSEE Journal of Power and Energy Systems*, 2(1):40–46, 2016.

[50] Mohamadreza Baradar, Mohammad Reza Hesamzadeh, and Mehrdad Ghandhari. Second-order cone programming for optimal power flow in VSC-type AC-DC grids. *IEEE Transactions on Power Systems*, 28(4):4282–4291, 2013.

[51] L. Gan and S.H. Low. Optimal power flow in direct current networks. *IEEE Transactions on Power Systems*, 29(6):2892–2904, 2014.

[52] Chee Wei Tan, Desmond W.H. Cai, and Xin Lou. Resistive network optimal power flow: Uniqueness and algorithms. *IEEE Transactions on Power Systems*, 30(1):263–273, 2015.

[53] Abbas Rabiee, Alireza Soroudi, and Andrew Keane. Information Gap Decision Theory Based OPF with HVDC Connected Wind Farms. *IEEE Transactions on Power Systems*, 30(6):3396–3406, 2015.

[54] Jun Cao, Wenjuan Du, Haifeng F. Wang, and S. Q. Bu. Minimization of transmission loss in meshed AC/DC grids with VSC-MTDC networks. *IEEE Transactions on Power Systems*, 28(3):3047–3055, 2013.

[55] Roger Wiget and Goran Andersson. Optimal power flow for combined AC and multi-terminal HVDC grids based on VSC converters. In *IEEE Power and Energy Society General Meeting*, 2012.

[56] Alejandro Pizano-Martinez, Claudio R. Fuerte-Esquivel, Hugo Ambriz-Pérez, and Enrique Acha. Modeling of VSC-based HVDC systems for a Newton-Raphson OPF algorithm. *IEEE Transactions on Power Systems*, 22(4):1794–1803, 2007.

[57] Somayeh Sojoudi, Ramtin Madani, and Javad Lavaei. Low-rank solution of convex relaxation for optimal power flow problem. *2013 IEEE International Conference on Smart Grid Communications, SmartGridComm 2013*, pages 636–641, 2013.

[58] Steven H. Low. Convex Relaxation of Optimal Power Flow—Part I: Formulations and Equivalence. *IEEE Transactions on Control of Network Systems*, 1(1):15–27, 2014.

[59] Shahab Bahrami, Francis Therrien, Vincent W.S. Wong, and Juri Jatskevich. Semidefinite Relaxation of Optimal Power Flow for AC-DC Grids. *IEEE Transactions on Power Systems*, 32(1):289–304, 2017.

[60] Steven H. Low. Convex relaxation of optimal power flow-part II: Exactness. *IEEE Transactions on Control of Network Systems*, 1(2):177–189, 2014.

[61] Javad Lavaei and Steven H. Low. Zero duality gap in optimal power flow problem. *IEEE Transactions on Power Systems*, 27(1):92–107, 2012.

[62] Niangjun Chen, Chee Wei Tan, and Tony Q.S. Quek. Electric vehicle charging in smart grid: Optimality and valley-filling algorithms. *IEEE Journal on Selected Topics in Signal Processing*, 8(6):1073–1083, 2014.

[63] Abimbola M. Jubril, Olusola A. Komolafe, and Kehinde O. Alawode. Solving multi-objective economic dispatch problem via semidefinite programming. *IEEE Transactions on Power Systems*, 28(3):2056–2064, 2013.

[64] Yunan Zhu, Jinbao Jian, Jiekang Wu, and Linfeng Yang. Global optimization of non-convex hydro-thermal coordination based on semidefinite programming. *IEEE Transactions on Power Systems*, 28(4):3720–3728, 2013.

[65] Emiliano Dall'Anese, Hao Zhu, and Georgios B. Giannakis. Distributed optimal power flow for smart microgrids. *IEEE Transactions on Smart Grid*, 4(3):1464–1475, 2013.

[66] Temesgen M. Haileselassie and Kjetil Uhlen. Impact of DC line voltage drops on power flow of MTDC using droop control. *IEEE Transactions on Power Systems*, 27(3):1441–1449, 2012.

[67] Wenyuan Wang, Student Member, Mike Barnes, and Senior Member. Power Flow Algorithms for Multi-Terminal VSC-HVDC With Droop Control. 29(4):1721–1730, 2014.

[68] Khaled Alshammari, Hasan Alrajhi Alsiraji, and Ramadan El Shatshat. Optimal Power Flow in Multi-Terminal HVDC Systems. *2018 IEEE Electrical Power and Energy Conference, EPEC 2018*, pages 1–6, 2018.